УДК 539.12.01

FINITE TEMPERATURE QCD ON THE LATTICE*
E.Laermann

Fakultät für Physik, Universität Bielefeld, Postfach 100 131,
33501 Bielefeld, Germany

FINITE TEMPERATURE QCD ON THE LATTICE*
E.Laermann

Fakultät für Physik, Universität Bielefeld, Postfach 100 131,
33501 Bielefeld, Germany

The article summarizes the current status of lattice investigations of Quantum Chromo Dynamics at finite temperature. After a brief introduction into the formulation of QCD on the lattice and into the treatment of lattice QCD in numerical simulations, the current knowledge about the critical temperature of the transition from the hadron to the quark gluon plasma phase is presented. The status of investigations of the nature of this transition is discussed. Moreover, analyses of the equation of state in the high temperature phase as well as computations of the excitation spectrum at nonvanishing temperature are presented.

В работе рассматривается современное состояние решеточных исследований КХД при конечной температуре. После обозрения формулировки и численного моделирования КХД на решетке рассмотрено современное представление о критической температуре перехода от адронной фазы к фазе кварк-глюонной плазмы. Обсуждается состояние исследований природы этого перехода. Кроме того, представлены как анализ уравнения состояния в высокотемпературной фазе, так и вычисления спектра возбуждений при конечной температуре.

1. INTRODUCTION

The transition from hadronic matter to a new state of matter, the quark gluon plasma, at some finite temperature T_c is a phenomenon which is governed by long range interactions. As such, its understanding requires a nonperturbative treatment of QCD. Due to the asymptotic freedom of QCD which predicts that the temperature dependent coupling $g(T)$ vanishes in the limit $T \to \infty$, at very high temperatures one expects only weakly interacting gas of quarks and gluons. However, it is not clear at which value of the temperature one may apply perturbation theory reliably. This holds, in particular, in the temperature regime which can be accessed by the forthcoming heavy ion collision experiments at RHIC and LHC. Moreover, finite temperature perturbative calculations are usually plagued by infrared divergencies which seem to be curable only nonperturbatively. Thus, nonperturbative analyses of QCD are also requested in order to obtain information on the properties of the plasma phase.

---

*Lectures presented at the "Research Workshop on Deconfinement at Finite Temperature and Density", Dubna, Russia, October 1–29, 1997

The lattice approach to QCD distinguishes itself from other nonperturbative treatments by the principal absence of any approximation to QCD. Of course, due to the ever present limitations of computational power to evaluate the QCD path integral numerically, systematic errors of lattice QCD arise from the necessary constraints on the lattice volume, the finite lattice spacing a and the quark mass. In particular, since the computations which take into account virtual quark loops are very time consuming, many lattice analyses have been carried out in the pure gauge sector of QCD, the quenched approximation. This has delivered nontrivial results as the pure glue system is confining and chiral symmetry breaking. In particular, bulk properties of gluons at finite temperature can be regarded as being solved: the system has a well-established first-order transition [1], the equation of state is known in the continuum limit [2], and the critical temperature in the continuum limit has been determined with only a few percent uncertainty [3,4]. Clearly, more detailed questions like, e.g., the nature of excitations in the plasma deserve further work, also in the quenched approximation. Yet, the emphasis of recent research has shifted towards studies of full QCD including staggered as well as Wilson quarks. These studies have not yet reached the quality of quenched simulations. In particular, the quark masses could not yet be tuned to their physical values. Moreover, at the moment these studies are carried out at considerably larger lattice spacings for technical reasons. Therefore, with the standard discretizations, extrapolations to the continuum limit (vanishing lattice spacing) will be more difficult than in the quenched case. Thus, the search for improved actions has received much attention recently also in the context of finite temperature QCD.

These lectures attempt to summarize the current status of knowledge in finite temperature lattice QCD and the current developments to improve on these results. In section 2 a short introduction into lattice techniques is given. Section 3 summarizes estimates of the critical temperature. In section 4 the present status of knowledge about the nature of the chiral transition is discussed. Section 5 describes studies of energy density and pressure at high temperature while section 6 reviews some results on screening lengths and masses. Conclusions are given in section 7.

2. LATTICE SIMULATIONS

The partition function $Z(V, T)$ of a generic Quantum Field Theory with elementary fields Φ in a given spatial volume V at temperature T is given by the path integral

$$Z(V, T) = \int \mathcal{D}\Phi \, e^{-S_E(V,T)}. \tag{1}$$

Here S_E is the Euclidean action, which defines the field theory in terms of a 4-dimensional integral over the Lagrangian, $\mathcal{L}$,

$$S_E(V,T) = \int_0^{1/T} dt \int_V d^3x \mathcal{L}(\Phi). \tag{2}$$

The Lagrangian depends only on the fundamental fields $\Phi(t,\vec{x})$ and a set of coupling constants. The temperature and volume of a thermodynamic system enter through the restriction of the fundamental fields to a finite (3+1)-dimensional region of space-time. In particular, the temperature enters by restricting the Euclidean time interval to the range $t \in [0,1/T]$ and by demanding periodic (antiperiodic) boundary conditions for bosonic (fermionic) fields in this direction. Thermodynamic quantities can then be obtained as derivatives of the partition function. For instance, the energy density and the pressure are given by

$$\epsilon = \frac{T^2}{V}\frac{\partial}{\partial T}\ln Z, \qquad p = T\frac{\partial}{\partial V}\ln Z. \tag{3}$$

The quantum field theory, defined formally by the above relations, can be regularized by introducing a discrete space-time lattice with a finite lattice spacing a. This spacing acts as a coordinate cut-off which has to be removed at the end, i.e., the continuum limit $a \to 0$ has to be taken. On the lattice, the number of degrees of freedom is reduced to a large but finite set. This gives a well defined statistical interpretation to the path integral and to most observables of interest, which can be viewed as expectation values calculated in a statistical ensemble with Boltzmann weights $\exp(-S_E)$.

On a 4-dimensional space-time lattice with a lattice spacing a, the fields $\Phi(x)$ are restricted to the discrete set of points, $(x_0,\vec{x}) \to na \equiv (n_0a, n_1a, n_2a, n_3a)$. Accordingly, $\Phi(x)$ gets replaced by $\phi(n)$ and the measure in the path integral $\mathcal{D}\Phi$ becomes $\prod_n d\phi(n)$. The partition function of this system reads

$$Z(V,T) = \int \prod_n d\phi(n)\, e^{-S_E(V,T)}, \tag{4}$$

where the temperature of a lattice of size $N_\tau \times N_\sigma^3$ is determined by the temporal extent, $T = 1/N_\tau a$, and the spatial volume is given by $V = (N_\sigma a)^3$.

The crucial step in formulating a lattice regularized quantum field theory is the proper discretization of the Euclidean action, S_E. This can be achieved in a straightforward way for a scalar field theory by discretizing the integral in Eq. (2) and replacing derivatives of fields by finite differences. The action of the ϕ^4-theory for instance, may be discretized as

$$\int d^4x \left\{ \frac{1}{2}\sum_\mu (\partial_\mu \Phi(x))^2 + \frac{1}{2}m^2\Phi^2(x) + \frac{g}{4!}\Phi^4(x) \right\} \to$$

$$\to \sum_{n=(n_0,..,n_3)} a^4 \left\{ -\frac{1}{a^2} \sum_{\mu=0}^{3} \phi(n)\phi(n+\hat{\mu}) + \frac{1}{2}(m^2 + \frac{8}{a^2})\phi^2(n) + \frac{g}{4!}\phi^4(n) \right\},$$
(5)

with $\hat{\mu}$ denoting the unit vector pointing to neighbouring sites in a 4-dimensional lattice, m being the particle mass and g the coupling constant.

In the case of a gauge theory the discretization is not at all so obvious. In fact, it is important to choose a discretization such that the basic symmetries of the continuum action are preserved. This is not always possible as, e.g., for fermionic theories. However, the most important step clearly is to construct a discretized action which preserves local gauge invariance [5].

Gauge fields mediate the interactions between matter. It is thus suggestive to introduce them as variables on the links (n,μ) of the lattice rather than on the sites. Gauge fields, $A_\mu(x)$, can then be related to elements $U_\mu(n)$ of a gauge group. In the case of an $SU(N)$ gauge theory, the relation between $U_\mu(n)$ and $A_\mu(x)$ is given by

$$U_\mu(n) = \exp\left[-iga \int_{na}^{na+\hat{\mu}a} \mathrm{d}x_\mu A_\mu(x)\right] ,$$
(6)

where g is the bare coupling constant. Expanding this relation in the lattice spacing one can verify that the single plaquette action proposed by Wilson [5]

$$S_G = \frac{2N}{g^2} \sum_{n;0\leq\mu<\nu\leq3} \square =$$

$$= \frac{2N}{g^2} \sum_{n;0\leq\mu<\nu\leq3} \frac{1}{N} Re\,\mathrm{tr}\, U_\mu(n)U_\nu(n+\hat{\mu})U_\mu^{-1}(n+\hat{\nu})U_\nu^{-1}(n) ,$$
(7)

approximates the continuum action for the gauge fields up to terms of $O(a^2)$,

$$S_G = \int \mathrm{d}^4x \frac{1}{2}\mathrm{tr}F_{\mu\nu}^2 + O(a^2).$$
(8)

In the continuum limit, $a \to 0$, these higher order corrections become irrelevant.

Wilson also suggested a discretization scheme for fermionic actions. While it is easy to preserve local gauge invariance also in this case, it is not possible to preserve all the chiral properties of fermionic actions. Fermion actions contain only first derivatives of the fields. As a consequence, a straightforward discretization, similar to the scalar case described in Eq. (5), leads to additional poles in the lattice fermion propagator. In the continuum limit these additional poles will give rise to 15 additional, unwanted fermion species rather than only the one we started with. It could be shown [6] that this is a general phenomenon when in addition to such elementary assumptions as locality, hermiticity and translational

invariance also a continuous chiral symmetry of the action is required. There are however certain loopholes. Wilson proposed a discretization scheme for fermions, in which a second-order derivative term is added to the naively discretized fermion action S_F,

$$S_F^{(W)} = \frac{1}{2}\sum_{n,\mu}\{\overline{\psi}(n)\gamma_\mu U_\mu(n)\psi(n+\hat{\mu}) - \overline{\psi}(n+\hat{\mu})\gamma_\mu U_\mu^{-1}(n)\psi(n)\} +$$

$$+ \frac{1}{2}\sum_{n,\mu}\{2\overline{\psi}(n)\psi(n) - \overline{\psi}(n+\hat{\mu})U_\mu^{-1}(n)\psi(n) - \overline{\psi}(n)U_\mu(n)\psi(n+\hat{\mu})\}. \quad (9)$$

While the first term approximates the continuum action $\overline{\psi}(x)[\partial_\mu + igA_\mu(x)]\psi(x) + \mathcal{O}(a^2)$, the second term is $O(a)$ relative to the first one and becomes irrelevant in the (naive) continuum limit. Its effect is that the 15 additional fermions acquire a large mass of $O(1/a)$, which diverges in the continuum limit, and thus would decouple from the dynamics of the theory. However, chiral invariance of the action is lost at finite lattice spacing and is to be recovered in the continuum limit. Usually, including a mass term, Wilson's fermion action is rewritten as

$$S_F^{(W)} = \overline{\psi}(n)\psi(n) -$$

$$- \kappa\sum_{n,\mu}\{\overline{\psi}(n)(1-\gamma_\mu)U_\mu(n)\psi(n+\hat{\mu}) + \overline{\psi}(n+\hat{\mu})(1+\gamma_\mu)U_\mu^{-1}(n)\psi(n)\}. \quad (10)$$

The hopping parameter κ contains the quark mass and, in the free case, is given by $\kappa^{-1} = 8 + 2m_q a$.

Another approach is due to Kogut and Susskind [7]. By distributing four components of the continuum spinor over different sites of the lattice it is possible to reduce the number of additional species. If one introduces one staggered fermion species on the lattice, the Kogut — Susskind or staggered lattice action will lead to $N_F = 4$ species of fermions in the continuum limit. Moreover it preserves a global $U(1) \times U(1)$ chiral symmetry, i.e., an Abelian subgroup of the continuum chiral symmetry. For studies of chiral symmetry breaking on the lattice it is convenient to work with such a lattice action which preserves at least part of the $SU(N_F) \times SU(N_F)$ chiral symmetry of the continuum action. The staggered fermion action, obtained after a diagonalization in the Dirac indices, becomes

$$S_F^{(KS)} = \sum_{n,l}\bar{\chi}(n)M(n,l)\chi(l). \quad (11)$$

Here the fermion fields, χ, $\bar{\chi}$, are single-component anticommuting Grassmann variables defined on the sites of the lattice and the fermion matrix $M(n,l)$ is given by

$$M(n,l) = \sum_{\mu=0}^{3} D_\mu(n,l) + m\delta(n,l). \quad (12)$$

The hopping matrices $D_\mu(n, l)$ mediate the nearest neighbour interactions and have nonzero elements only for $l = n \pm \hat{\mu}$,

$$D_\mu(n, l) = \frac{1}{2}\eta_\mu(n)[U_\mu(n)\delta(n + \hat{\mu}, l) - U_\mu^{-1}(l)\delta(n - \hat{\mu}, l)]. \qquad (13)$$

The phase factors $\eta_\mu(n) = (-1)^{n_0 + \dots + n_{\mu-1}}$ for $\mu > 0$ and $\eta_0(n) = 1$ are remnants of the γ_μ matrices. Note that the fermion action in the Wilson discretization, Eq. (9) can be written in a similar form with a slightly more complicated hopping term which also carries spinor indices.

Finally, the partition function of QCD takes on the form

$$Z = \int \prod_{n,\mu} dU_\mu(n) \prod_n d\chi(n)d\bar{\chi}(n)\, e^{-\left[S_G + S_F\right]}, \qquad (14)$$

where for Wilson's formulation the χ fields are to be replaced by the ψ spinors. As the fermionic part of the action is bilinear in the fields $\bar{\chi}(n)$, $\chi(n)$, these can be integrated out and the partition function can be represented in terms of bosonic degrees of freedom only,

$$Z = \int \prod_{n,\mu} dU_{n,\mu} \det M\, e^{-S_G}. \qquad (15)$$

In this form the partition function is well suited for numerical studies. A major problem is, however, caused by the presence of the fermion determinant, which in general cannot be calculated exactly. Algorithms for the numerical integration, which circumvent the explicit calculation of this determinant, are thus required.

In the lattice regularization, the Feynman path integral, Eq. (4), becomes a well-defined meaning as an ordinary integral. Because of the high dimensionality, its numerical evaluation, however, is a formidable task. Imagine a lattice of just 10^4 lattice points, then Eq. (4) represents a 10^4 fold integral times the number of internal degrees of freedom. Many field configurations $\{\phi\}$ will contribute to the integral with rather small Boltzmann weights, $\exp\{-S(\phi)\}$, though. Thus an efficient way to compute the integral would consist in generating a sequence of field configurations $\{\phi\}^{(k)}$ which are distributed according to this weight factor. The expectation value of an observable $\mathcal{O}(\phi)$ can then be approximated by the ensemble average

$$\langle \mathcal{O}(\phi) \rangle = \frac{1}{M} \sum_{k=1}^{M} \mathcal{O}(\{\phi\}^{(k)}). \qquad (16)$$

Such a series of field configurations is obtained by means of the so-called Markov chains. Starting from some arbitrary initial configuration $\{\phi\}^{(0)}$ one generates, one after the other, new sets of ϕ fields. Under certain conditions, the sets $\{\phi\}^{(k)}$

will be distributed according to the equilibrium probability $\exp\{-S(\phi)\}$, once a number of not-yet equilibrated initial configurations has been discarded.

It may suffice here to demonstrate the principles of this procedure by presenting the prototype Metropolis algorithm [8]. It consists of two steps: site by site (i) choose a trial update ϕ' according to some normalized probability distribution $P_{trial}(\phi \to \phi') = P_{trial}(\phi' \to \phi)$ and (ii) accept ϕ' with the conditional probability

$$P_{accept} = \min\left\{1, \frac{e^{-S(\phi')}}{e^{-S(\phi)}}\right\}. \qquad (17)$$

The trial distribution P_{trial} must be chosen in such a way that the whole configuration space can be covered. The conditional accept probability P_{accept} favors configurations with lower action and thus higher Boltzmann weight but allows also for configurations with a smaller Boltzmann weight to be included in the set. This is necessary in order to account for the quantum fluctuations. Finally, the algorithm satisfies detailed balance, $(P = P_{trial} * P_{accept})$

$$e^{-S(\phi)}P(\phi \to \phi') = e^{-S(\phi')}P(\phi' \to \phi), \qquad (18)$$

which is a sufficient condition for convergence to the equilibrium distribution.

As new configurations are calculated from previous ones, it is clear that subsequent "snapshots" of the system are not statistically independent of each other. In order to carry out a correct statistical error analysis it is therefore desirable to step through configuration space rather quickly, minimizing the number of intermediate configurations which have to be discarded because they do not provide information independent of the previous state. The Metropolis algorithm is local and can be implemented efficiently. However, either the new value ϕ' is close to the old one, in which case the change in the action is small and its acceptance is likely, or the new ϕ' is far from the old one. In the latter case the change in the action is large, however, and the acceptance rate drops exponentially. Both choices result in a slow exploration of configuration space. These autocorrelation times between subsequent configurations can in general be decreased by using algorithms which mix stochastic updatings with deterministic ones.

In the full theory, with dynamical fermions, one has to deal with the fermion determinant, Eq. (15). Here, most simulations make use of the hybrid Monte Carlo algorithm [9, 10]. As a prerequisit the determinant is re-expressed by a path integral over pseudofermion fields, i.e., bosonic (commuting) fields which interact via the inverse fermion matrix*,

$$\det\{D + m\} = \int \prod_n d\phi(n)d\phi^*(n) \exp\{-\phi^*(D+m)^{-1}\phi\}. \qquad (19)$$

---

*As the fermion matrix is not positive definite, one first has to square the determinant in order to obtain a regular Boltzmann weight factor. This minor complication will be neglected in the following.

Because of the nonlocality of the inverse Dirac matrix, any local updating scheme for the gauge fields in Eq. (15) would though require to recalculate the inverse after each local change in the U's. Alternatively, one could change a whole gauge field configuration at once and then recalculate the inverse. However, with ordinary, local updating procedures, the acceptance probability of a global change would drop to zero very quickly with the lattice size. The hybrid Monte Carlo algorithm solves this problem by deliberately preparing a new configuration for a global accept/reject decision, Eq. (17). For this purpose one adds a quadratic term to the action,

$$\mathcal{H} = \frac{1}{2} \sum_{n,\mu} \mathrm{tr} \pi_\mu^2(n) + S_G(U) + \phi^*(D+m)^{-1}\phi \ ,\tag{20}$$

which can be integrated out analytically and does not change expectation values. This expression, Eq. (20), is now taken as a Hamiltonian, with $\pi_\mu(n)$ being the momenta conjugate to the gauge fields, from which the Hamiltonian equations of motion* in a fictitious time τ are derived [11],

$$\begin{aligned} \frac{d}{d\tau}U_\mu(n) &= i\pi_\mu(n)U_\mu(n) \\ i\frac{d}{d\tau}\pi_\mu(n) &= U_\mu(n)\frac{\partial}{\partial U_\mu(n)}\mathcal{H}. \end{aligned}\tag{21}$$

By numerically integrating the Hamilton equations over some time interval the whole of the gauge fields are evolved relatively fast through phase space. Since Hamilton's equations are energy conserving, $\mathcal{H} = \mathrm{const}$, the new values for the gauge fields would be accepted with probability 1 if one could do the integration exactly. Discretization errors, however, cause slight violations of energy conservation which are corrected for in a global Metropolis acceptance decision, Eq. (17). By controlling the discretization step width $d\tau$ one can keep the energy conservation violations small and maintain a large acceptance probability. Finally, the molecular dynamics evolution, Eq. (21), is supplemented by random refreshments of the momenta π and the pseudofermions ϕ in order to guarantee ergodicity.

   In simulations with dynamical fermions, by far the largest fraction of computing time goes into repeatedly calculating the inverse of the Dirac matrix. For that purpose, solvers which iteratively explore the Krylov space like, e.g., the conjugate gradient algorithm are used [12]. The numerical effort for the inversion

---

*Eq. (21) represents a slight modification of Hamilton's equations in order to preserve the gauge fields as elements of the gauge group.

depends on the fermion mass via the condition number,

$$\frac{|\lambda|_{max}}{|\lambda|_{min}} \sim \frac{1}{m} \quad , \tag{22}$$

where λ denotes an eigenvalue of the Dirac matrix. This explains the high cost of simulations with small fermion masses.

As the numerical effort required for the simulation of fermions is quite large, many lattice investigations have been using the so-called quenched approximation. This approximation amounts to setting the determinant equal to 1,

$$\det\{D + m\} = \exp\left[\operatorname{tr}\log(D + m)\right] \overset{!}{=} 1. \tag{23}$$

Expanding the exponent leads to

$$\operatorname{tr}\log(D + m) \sim \sum_{k=0}^{\infty} (\frac{1}{m})^{2k} \operatorname{tr} D^{2k} \overset{!}{=} 0. \tag{24}$$

The Dirac matrix D connects neighbouring lattice sites via a gauge link and in a way describes the hopping of a fermion from one site to the next. Because of the trace, only closed loops contribute in Eq. (24). Thus, the seemingly crude quenched approximation amounts to neglecting virtual quark loops and treats fermions as static degrees of freedom. Properties of the theory which depend crucially on the fermion dynamics are thus not accessible by studies in the quenched approximation. On the other hand, basic properties of QCD which are dominated by the non-abelian gluon dynamics should and do survive the approximation. Quenched studies therefore serve as important guides for many nonperturbative aspects of the theory. Of course, the results have to be checked by calculations in the full theory.

The statistical accuracy of computations notably in the quenched approximation has nowadays become so good that the major uncertainty of the results is the systematic error arising from finite lattice spacings. There are attempts to reduce this error by using the so-called improved actions. A detailed presentation of this rather technical issue is beyond the scope of these lectures, yet it might be useful to demonstrate some ideas.

Improved actions are targeted at reducing the deviations between the continuum and the lattice action to higher orders in the lattice spacing. In principle, e.g., for a generic scalar action, this can be achieved by using better finite difference approximants to the derivative. With

$$\begin{aligned}
S_1 &= \frac{1}{2a}\left[\phi(x + \hat{\mu}) - \phi(x - \hat{\mu})\right] &=& \partial_\mu\phi + \frac{a^2}{6}\partial_\mu^3\phi + \mathcal{O}(a^4) \\
S_2 &= \frac{1}{6a}\left[\phi(x + 3\hat{\mu}) - \phi(x - 3\hat{\mu})\right] &=& \partial_\mu\phi + \frac{3a^2}{2}\partial_\mu^3\phi + \mathcal{O}(a^4)
\end{aligned} \tag{25}$$

one obtains

$$\frac{9}{8}S_1 - \frac{1}{8}S_2 = \partial_\mu \phi + \mathcal{O}(a^4) \tag{26}$$

and thus reduces the deviations from $\mathcal{O}(a^2)$ to $\mathcal{O}(a^4)$. Clearly, this procedure is not unique and can be iterated towards increasingly better approximants. The price to be paid are successively more extended lattice operators and correspondingly more computational effort per lattice site. The same principle applies to gauge fields although the generalization is perhaps not so immediate because gauge invariance ought to be preserved. Here one adds larger loops to the simple plaquette term, Eq. (7), in the simplest case

$$S_G \sim \frac{4}{3} \boxed{} - \frac{1}{6} \boxed{} \sim S_G^{\text{cont}} + \mathcal{O}(a^4). \tag{27}$$

The coefficients of the two loops have been adjusted at tree level so as to improve the classical action. In the path integral, however, quantum corrections introduce deviations of order $a^2 g^{2n}$. In principle [13] these can be eliminated order by order in perturbation theory. For on-shell quantities this program was carried out at one-loop level [14]. However, lattice perturbation theory in the bare gauge coupling is badly converging in the parameter range usually explored in numerical studies. The bad convergence can be traced back to the expansion of the link variable U_μ, Eq. (6), in terms of the gauge potential A_μ,

$$U_\mu \simeq 1 + iagA_\mu - \frac{1}{2}a^2 g^2 A_\mu^2 + ... \tag{28}$$

The higher orders lead to vertices not present in continuum perturbation theory. Their contributions are not small at gauge couplings of $\mathcal{O}(1)$. Moreover, they lead to "tadpole" diagrams [15] which enhance $\mathcal{O}(a^2 g^{2n})$ corrections to $\mathcal{O}(g^{2n})$. These unwanted terms can partly be eliminated by the so-called tadpole improvement. In this approach the link variables are renormalized by their mean field value (which in the lowest nontrivial order is given by the tadpole contribution) and the perturbative series is carried out in a renormalized coupling. It is however *a priori* not known whether nonperturbative quantities are sufficiently improved by this recipe.

Similar improvement programs have been suggested for fermion actions [16, 17]. This seems important in particular for the Wilson discretization which deviates from the continuum action in $\mathcal{O}(a)$, compared to staggered fermions at $\mathcal{O}(a^2)$. Here, also a nonperturbative determination of the coefficients in the action by requiring certain Ward identities to hold have been advocated [18] and are being explored.

Finally, renormalization group ideas have been used to construct improved actions [19]. Integrating out high momentum fluctuations leads to coarse grained lattices and defines a renormalization group flow in a multidimensional parameter

space. In principle one could thus derive a perfect action which at a given value for the lattice spacing "sits" on the renormalized trajectory. In practice one has to truncate the set of different lattice operators to some manageable number. Again, this approach is also being used and tested.

3. CRITICAL TEMPERATURE

One of the basic quantities to be derived from finite temperature lattice QCD is the value of the critical temperature. The critical temperature is obtained from the location where a certain order parameter vanishes. In the case of the pure $SU(N)$ gauge theory this order parameter is the expectation value of the Polyakov loop

$$\langle L \rangle = \langle \frac{1}{N} \text{tr} \prod_{n_0=1}^{N_\tau} U_0(n_0) \rangle. \tag{29}$$

Below the phase transition its vanishing signals that the theory is invariant under the center symmetry $Z(N)$ of $SU(N)$: $U_0(N_\tau) \to zU_0(N_\tau)$ with $z\epsilon Z(N)$. Above T_c the finite value of $\langle L \rangle$ shows breakdown of that symmetry. Moreover, the Polyakov loop is related to the free energy F_q of a single quark

$$\langle L \rangle = \exp(-F_q/T) \tag{30}$$

so that $\langle L \rangle = 0$ below T_c is equivalent to an infinite F_q, i.e., one has confinement. Above the transition, F_q can be finite because of deconfinement, hence $\langle L \rangle \neq 0$.

The fermionic part of the action breaks the center symmetry explicitly. Thus the Polyakov loop is not an order parameter in the symmetry sense anymore. The relation with the free energy still holds. However, in the chiral limit the QCD Lagrangian is invariant under chiral flavor transformations. These symmetries are spontaneously broken at $T = 0$ leading to a nonvanishing chiral condensate, $\langle \overline{\psi}\psi \rangle \neq 0$, and to massless Goldstone bosons, the pions. At high temperature one expects that the chiral invariance is restored indicated by $\langle \overline{\psi}\psi \rangle \to 0$ at the critical temperature.

Because on a finite lattice the Polyakov loop can tunnel through all different $Z(N)$ vacua one usually analyzes $\langle |L| \rangle$. In simulations with fermions one cannot run at vanishing quark mass. Both leads to nonvanishing tails of the order parameters in the "other" phase. Therefore, the corresponding susceptibilities $\chi_L = \langle |L|^2 \rangle - \langle |L| \rangle^2$ and $\chi_m = \langle (\overline{\psi}\psi)^2 \rangle - \langle \overline{\psi}\psi \rangle^2$ are more sensitive to the location of the critical temperature where they develop a peak.

In Fig.1 the Polyakov loop and the chiral condensate as well as the corresponding susceptibilities are plotted as a function of the coupling. The data originates from a simulation with two flavors of dynamical staggered quarks. Note that in principle the deconfinement and the chiral transition are two different
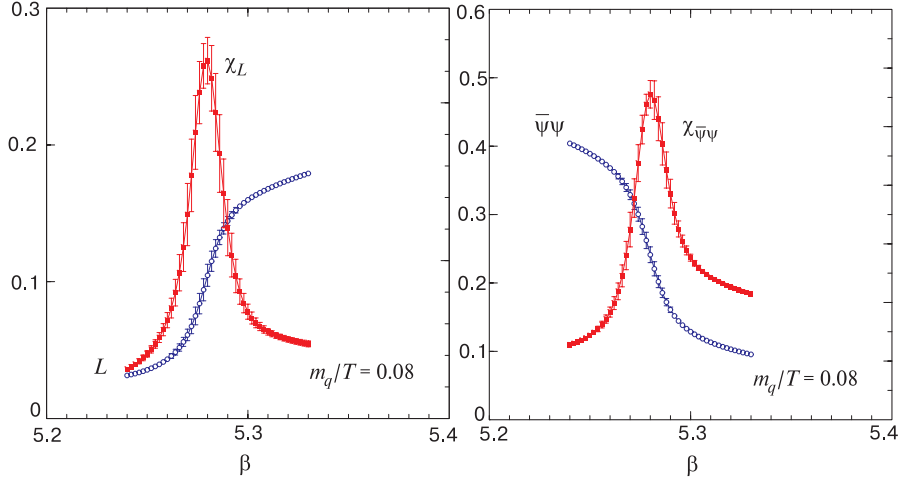
Fig. 1. Polyakov loop and chiral condensate together with the corresponding susceptibilities as a function of the coupling $\beta = 6/g^2$ from a simulation with two flavors of dynamical staggered quarks

phenomena, yet, one observes the peaks in both susceptibilities (with fermions in the fundamental color representation) at the same location.

Once the critical bare coupling is known, one needs to turn that value into a physical number for the temperature. Recall that the temperature of a lattice is given by the relation $T = 1/(N_\tau a(\beta))$ where the lattice spacing is dependent on the bare coupling $\beta = 6/g^2$ by dimensional transmutation. In order to vary T one can change N_τ in discrete steps or tune a by varying β. For each N_τ one needs a different value for a hence for β to tune to the same temperature. For a physical value of T or T_c a physical number for the lattice spacing has to be known. This is obtained by computing a quantity with nontrivial dimension like, e.g., a hadron mass m_H or the string tension σ on a lattice with the same bare coupling but at $T = 0$. This yields these quantities in lattice units, e.g., $\sigma_{\text{lat}} = \sigma a^2(\beta)$. In ratios like $T_c/\sqrt{\sigma} = 1/(N_\tau \sqrt{\sigma_{\text{lat}}})$ the lattice spacing drops out and the ratios should become independent of a. Due to nonuniversal scaling, i.e., an observable-dependent relation between a and β and due to lattice discretization effects these ratios need not be constant however. To obtain continuum numbers one has to extrapolate to $a \to 0$.

Figure 2 summarizes the current status of analysis in the quenched approximation. It shows the ratio $T_c/\sqrt{\sigma}$ for various actions where σ is the string tension extracted from the static quark potential at $T = 0$. For all data points the value of the critical coupling has been extrapolated to its infinite (spatial) volume limit at which then the string tension was determined. The lowest set
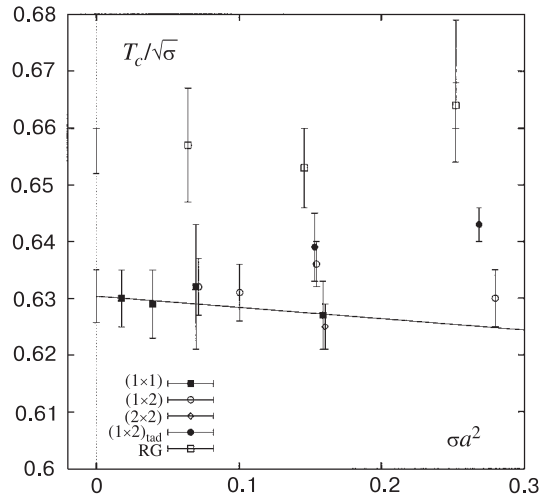
Fig. 2. The quenched critical temperature in units of the square root of the string tension for various gauge actions versus the lattice spacing squared
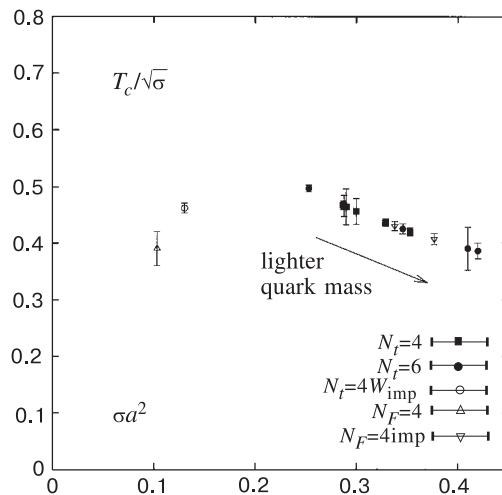

Fig. 3. The critical temperature in units of the square root of the string tension for dynamical fermions versus the square of the lattice spacing (for further explanations see text)

of data points originates from simulations with the standard Wilson gauge action [2,4]. An extrapolation in the lattice spacing to the continuum limit gives $T_c/\sqrt{\sigma} = 0.630(5)$. The data is compared with results from simulations with a variety of Symanzik-improved actions [4,21]. Note that in this particular ratio, $T_c/\sqrt{\sigma}$, no strong cut-off dependence is seen in neither case. Also the continuum
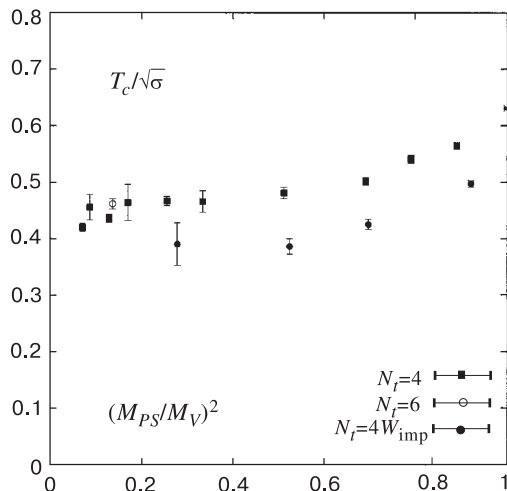
Fig. 4. The critical temperature in units of the square root of the string tension for dynamical fermions plotted versus $(M_{PS}/M_V)^2$. The point at $(M_{PS}/M_V)^2 = 1$ is the $N_\tau = 4$ quenched value

extrapolations are in agreement with each other. Likewise, the results [3] from Iwasaki's RG-improved action are consistent with a constant behavior in a, but they deliver a value of the critical temperature of $T_c/\sqrt{\sigma} = 0.656(4)$ which is about 3% higher than the number from the standard action. Since the procedure to extract the string tension has not been the same for the two numbers, one might suspect that the difference in the quoted values for T_c, $T_c = 276(2)$MeV versus 266(2) MeV, is mainly due to differences in the analysis of the static quark potential [22] rather than to differences in the improvement scheme.

The current situation with dynamical fermions is depicted in Fig.3. The plot summarizes data from simulations with 2 flavors of quarks, staggered fermions at $N_\tau = 4$ and 6 [23, 24] as well as improved Wilson fermions at $N_\tau = 4$ [23], plus $N_F = 4$ staggered results obtained from $N_\tau = 4$ lattices with an improved action [25] in addition to an old number [26] from $N_\tau = 8$ and a standard action. Compared to the equivalent quenched plot, Figure 3 shows that the lattice spacings at which T_c has been determined so far are considerably larger than in pure gauge theory simulations. Moreover, the investigations have not been carried out at the physical quark masses. The arrow in Figure 3 indicates that at fixed N_τ the transition takes place at larger lattice spacings when the quark mass is decreased. Thus the critical temperature is decreasing when the quark mass is lowered.

The same data is shown again in Fig.4 as a function of the pseudoscalar Goldstone boson to vector meson mass ratio $(M_{PS}/M_V)^2$ which is proportional
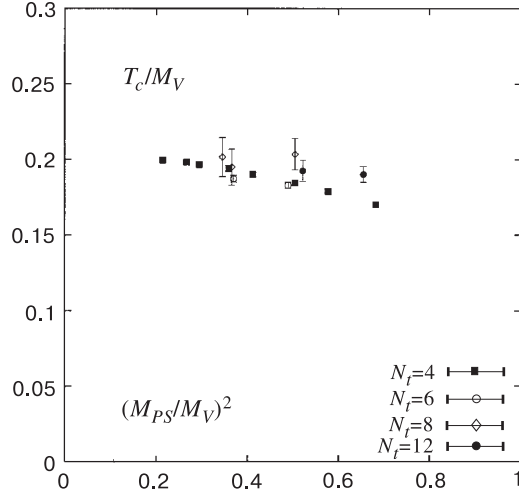
Fig. 5. The critical temperature in units of the vector meson mass for staggered fermions plotted versus $(M_{PS}/M_V)^2$

to the physical quark mass. Here now, at fixed N_τ, smaller lattice spacings are to the right of the figure. The $N_\tau = 4$ staggered data indicate that T_c over $\sqrt{\sigma}$ tends to lower values as the quark mass decreases. The same trend is observed for the Wilson improved results, although at larger $(M_{PS}/M_V)^2$ ratios. On the other hand, the $N_\tau = 6$ data point seems to indicate that, at a given quark mass, decreasing of the lattice spacing increases $T_c/\sqrt{\sigma}$ only slightly. At the moment, one would therefore estimate a physical value for the critical temperature of $T_c/\sqrt{\sigma} \lesssim 0.4$ or $T_c \lesssim 170$ MeV.

The critical temperature has also been estimated from the ratio to the vector meson mass. In this case one ought to go (close) to the chiral limit in order to extract a physical number because the vector meson mass depends on the quark mass. In the case of using the string tension to set the scale one might argue that the string tension is considerably less affected by the quark mass. Figure 5 shows T_c/M_V for $N_F = 2$ staggered fermions [24, 27–31], plotted as function of $(M_{PS}/M_V)^2$. As the quark mass is decreased this ratio rises. Recall that the infinite quark mass, quenched data point corresponds to $M_{PS}/M_V = 1$ and $T_c/M_V = 0$. As the lattice spacing is decreased, T_c/M_V stays remarkably constant. Extrapolating the $N_\tau = 4$ data to the chiral limit suggests a value of $T_c/M_V \simeq 0.2$ or $T_c \simeq 150$ MeV. Note that this value disagrees somewhat with the number extracted from the string tension.

The corresponding data for dynamical Wilson quarks [23, 32–34] are given in Fig.6. Although some unexpected crossover behavior at the critical temperature
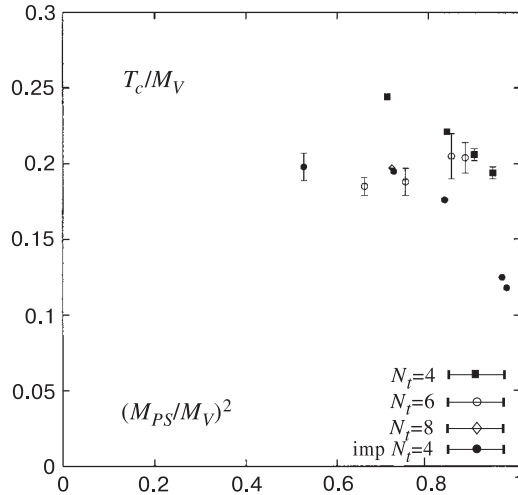
Fig. 6. The critical temperature in units of the vector meson mass for Wilson fermions versus $(M_{PS}/M_V)^2$

was observed with the standard Wilson fermion action, at least the results for $N_\tau = 6$ and 8 as well as the first data with improved Wilson fermions [23] are not in disagreement with the staggered data.

In summary, studies with dynamical fermions consistently have lead to an estimate of the critical temperature of order 150 MeV for 2 flavors so far. This value is considerably lower than the quenched number of $T_c = 270(5)$MeV. Because of the relation $T = 1/(aN_\tau)$ of the temperature T to lattice spacing a and temporal extent N_τ of the lattice, dynamical fermion simulations in the vicinity of the transition are correspondingly, at a given N_τ, carried out at considerably larger lattice spacings.

4. PHASE TRANSITION

The studies presented in this section are aiming at establishing the order of the transition to the plasma phase. A first order transition has discontinuities at the "critical" temperature, e.g., a latent heat, and the two phases are coexisting at T_c. At a second order transition the correlation length and certain response functions diverge while other quantities show a continuous behavior. These differences lead to observable consequences in the cooling of the early universe as well as in heavy ion collision experiments.

In the quenched approximation it has been clarified that the deconfinement transition is of first order [1]. In the full theory the nature of the transition is a

subject of active research. The most advanced studies so far have concentrated on two flavors of light quarks as one is expecting that the restoration of chiral symmetry is the important phenomenon also in the realistic case of two light, up and down quarks plus the heavier strange quark.

4.1. Staggered $N_F = 2$**: Critical Behavior.** The theoretical expectations on the scaling behavior of QCD at the chiral transition are based on the σ model in three dimensions. For the case of two light flavors, if the transition is of second order, it is expected to show scaling behavior with $SU(2) \times SU(2) \simeq O(4)$ exponents. On the other hand, if the anomalous $U_A(1)$ symmetry were effectively restored, the relevant symmetry group would be $U_A(1) \times SU(2) \times SU(2) \simeq O(2) \times O(4)$ and the transition could be of first order [35].

It has been attempted to analyze the critical behavior of two flavor staggered QCD by studying the scaling behavior of various quantities and determining critical exponents [36]. These scaling relations are derived from the scaling of the singular part of the free energy density under an arbitrary change of scale b,

$$f(t,h) = -\frac{T}{V} \ln Z = b^{-1} f(b^{y_t} t, b^{y_h} h). \tag{31}$$

Here, t is the reduced temperature, $t = (T - T_c)/T_c$, with T_c as the critical temperature in the chiral limit, and h is the symmetry breaking field, $h = m/T$. In the vicinity of the critical point, thermodynamic quantities should be governed by the thermal (y_t) and the magnetic (y_h) critical exponent. In the staggered version of lattice regularized QCD, for the dimensionless couplings t and h one uses

$$\begin{aligned} t &= \frac{6}{g^2} - \frac{6}{g_c^2(0)} \\ h &= maN_\tau, \end{aligned} \tag{32}$$

where $g_c(0)$ denotes the critical coupling on a lattice with fixed temporal extent in the limit of vanishing quark mass. At nonvanishing quark mass, a pseudo-critical coupling $g_c(m)$ is defined as the location of a peak in, e.g., the Polyakov loop susceptibility.

Quantities from which one can extract critical exponents are various susceptibilities, in particular, the magnetic or chiral susceptibility

$$\chi_m = \frac{T}{V} \sum_{i=1}^{N_F} \frac{\partial^2}{\partial m_i^2} \ln Z \tag{33}$$

and the thermal susceptibility

$$\chi_t = -\frac{T}{V} \sum_{i=1}^{N_F} \frac{\partial^2}{\partial m_i \partial(1/T)} \ln Z. \tag{34}$$

Table. Critical exponents for $O(2), O(4)$ and mean field (MF). The numerical 2 flavor QCD results are given separately for each spatial lattice size, with upper values denoting the JLQCD and the lower ones — the Bielefeld group numbers [40, 41]

	O(2)	O(4)	MF	L=8	L=12	L=16
z_g	0.60	0.54	2/3	0.70(11)	0.74(6)	0.64(5)
					0.63(6)	
z_m	0.79	0.79	2/3	0.70(4)	0.99(8)	1.03(9)
				0.84(5)	1.06(7)	0.93(8)
z_t	0.39	0.34	1/3	0.47(5)	0.81(9)	0.83(12)
				0.63(7)	0.94(12)	0.85(12)

Assuming that the free energy is dominated by its singular part, Eq. (31) then leads to the scaling predictions for the peak heights of the susceptibilities at the line of pseudocritical couplings

$$\chi_m^{\text{peak}} \sim m^{-z_m}$$
$$\chi_t^{\text{peak}} \sim m^{-z_t}, \tag{35}$$

where the exponents are given by $z_m = 2 - 1/y_h$ and $z_t = (y_t - 1)/y_h + 1$. The pseudocritical line itself is expected to follow

$$\frac{6}{g_c^2(m)} = \frac{6}{g_c^2(0)} + c\,m^{z_g} \tag{36}$$

with $z_g = y_t/y_h$. The values of these exponents for various symmetries [37] are given in the Table. At finite lattice spacing the exact chiral symmetry of the staggered fermion action is $U(1) \simeq O(2)$. However, sufficiently close to the continuum limit one expects $O(4)$ exponents. The possibility of mean-field (MF) exponents arbitrarily close to the transition has been raised by [38].

Earlier investigations of the exponents on small lattices ($8^3 \times 4$) had observed partial agreement with $O(4)$ scaling [39]. These studies have been repeated on larger spatial volumes, $L = 12, 16$ by the JLQCD collaboration [40] and by the Bielefeld group [41]. In addition to the quark mass values 0.02, 0.0375 and 0.075 in lattice units JLQCD also ran at $m = 0.01$. The volume dependence of the chiral susceptibility at peak is shown in Fig.7, similar results are available for the other quantities. For $m \geq 0.02$, the susceptibility rises when the volume is increased from 8^3 to 12^3, but then stays approximately constant. Thus, a phase transition does not occur in this mass range, in agreement with earlier claims [42]. At $m = 0.01$ the linear increase in the peak height as the volume is enlarged continues up to $L = 16$. As such, this observation could suggest a first order transition. JLQCD however have studied the volume dependence of a double-peak structure in the distribution of the chiral order parameter and conclude that a first order transition is likely to be absent [40].
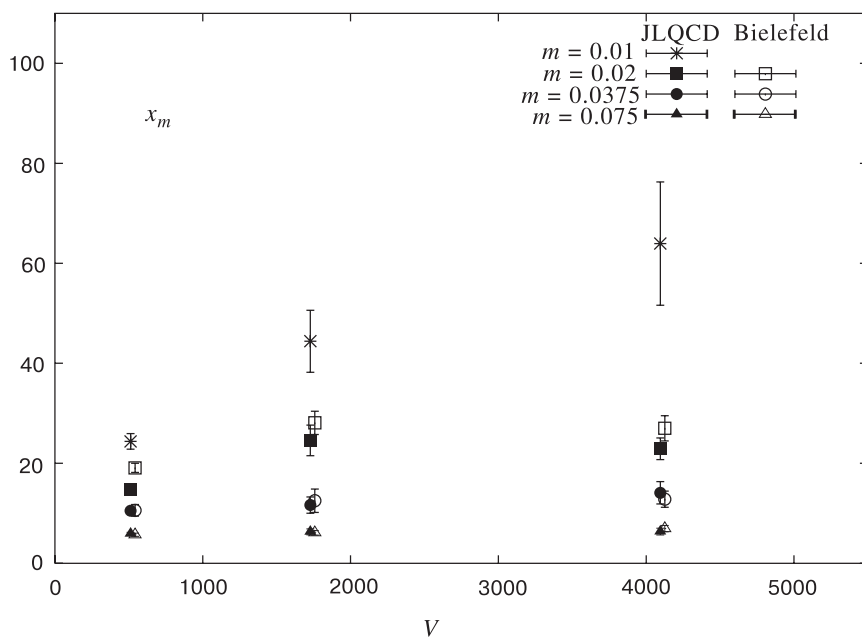
Fig. 7. Volume dependence of the chiral susceptibility χ_m at peak for two flavors of staggered quarks

The quark mass dependence of χ_m^{peak} is shown in Fig.8, expected scaling behavior, Eq. (35). The resulting values for the critical exponents are also summarized in the Table. For z_g, within two standard deviations, agreement with all three predictions is obtained. For the other two exponents, both groups consistently observe a drastic change when the spatial extent is increased from $L = 8$ to $L = 12, 16$. While for the small volume the value for z_m is in rough agreement with $O(2)$ and $O(4)$, the results from $L = 12$ and 16 do not agree with any of the predicted numbers. Indeed, the observed value $z_m \simeq 1$ would be expected for a first order transition. The thermal exponent z_t is larger than any of the predictions for all volumes.

Another way to study the scaling behavior is to compute the (magnetic) equation of state [43]

$$\langle \overline{\psi}\psi \rangle h^{-1/\delta} = \phi(th^{-1/\beta\delta}), \tag{37}$$

where the critical exponents δ and $\beta\delta$ are related to y_t and y_h as $1/\delta = 1/y_h - 1$ and $1/\beta\delta = y_t/y_h$. The scaling function ϕ was determined from a parametrization of $O(4)$ simulation results [44] and is universal, except that two nonuniversal normalization constants have to be adjusted. This has been done by the MILC
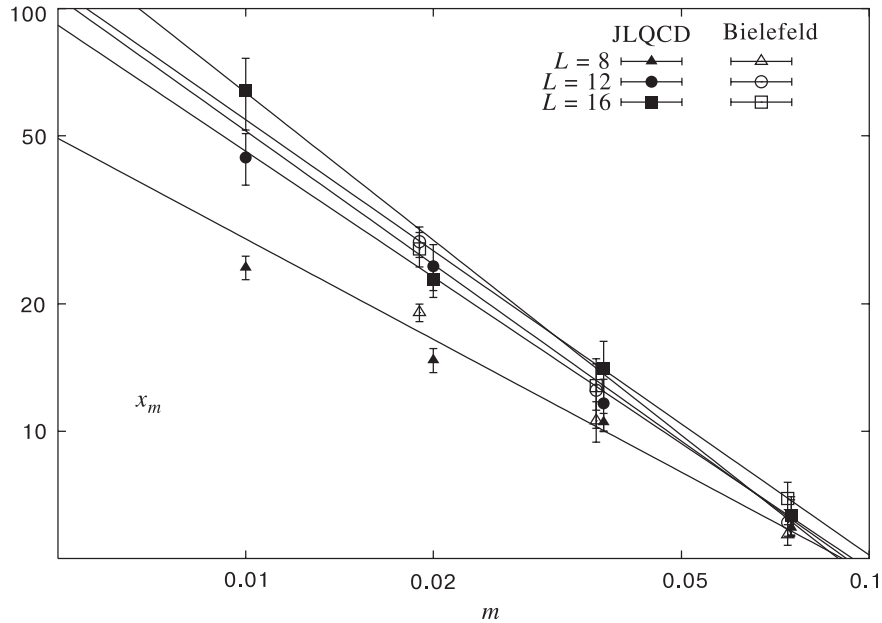
Fig. 8. Mass dependence of the chiral susceptibility χ_m at peak. The upper 4 lines are fit results with Eq. (35) to the $N_\sigma = L = 12$ and 16 data while the lowest line shows the slope of $O(4)$ scaling

Collaboration [45] for $N_\tau = 4, 6, 8$ and 12. The results are shown in Fig.9. While at $N_\tau = 4$ the data for the larger quark masses and smaller volumes are compatible with $O(4)$, the new data at smaller quark masses and larger lattice extent again show drastic disagreement. When N_τ is increased, thus going to smaller lattice spacings, the agreement becomes increasingly better [45], but it should be remarked that the data at $N_\tau = 12$ originates from physical quark mass values $m/T \simeq 0.1$ which are of about the same size as the larger quark masses used at $N_\tau = 4$. Also, even at large spacing one would expect $O(2)$ behavior which is indistinguishable from $O(4)$ with the current precision of the data.

At the moment there is no convincing explanation for these discrepancies at hand. In view of the results presented in section 4.3 obtained with an improved gauge action and Wilson fermions one might speculate that at strong coupling and for the standard action the relation between the QCD parameters and the thermodynamic variables, Eq. (32), as they enter the singular part of the free energy is strongly distorted. More studies at weaker coupling or with improved actions would be needed to solve this important question.
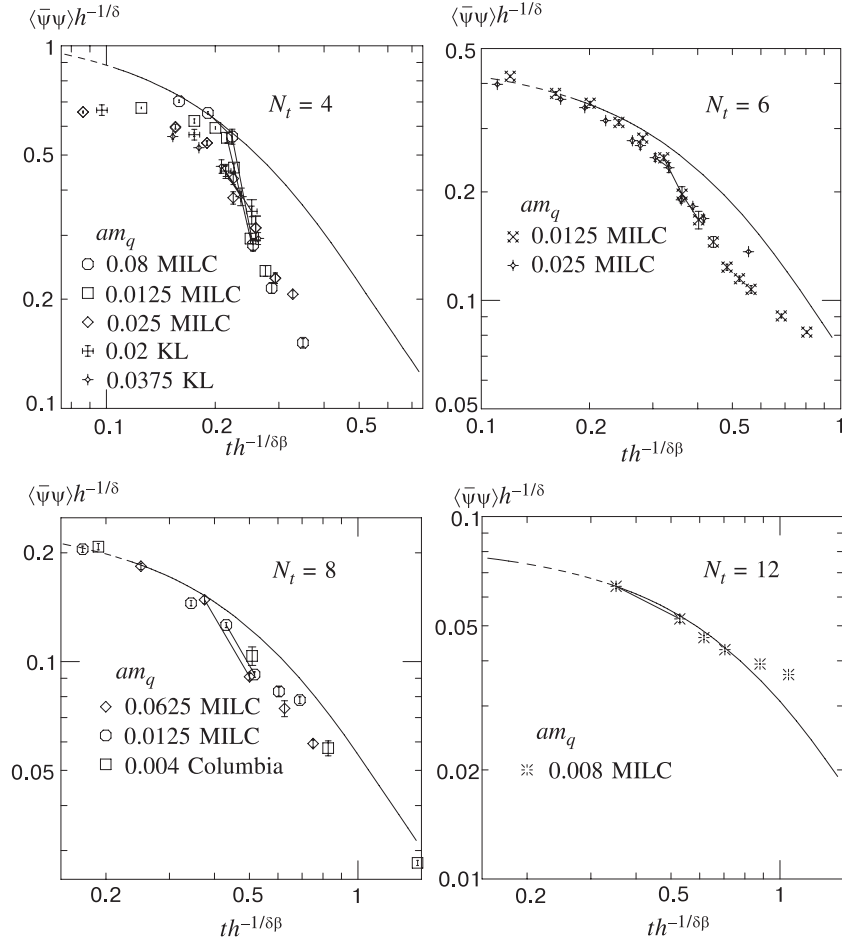
Fig. 9. The magnetic equation of state, Eq. (37), for $N_t = 4, 6, 8$ and 12 [45]. The line in each plot is the $O(4)$ scaling prediction. It can be moved horizontally as well as vertically by adjusting two free normalization constants

4.2. $U_A(1)$ Restoration. The nature of the chiral transition for two flavors is strongly affected by the realization of the $U_A(1)$ symmetry [35]. This symmetry is present in the classical continuum action but is destroyed by the famous triangle anomaly. At very high temperatures topologically nontrivial configurations are suppressed. This could lead to the effective restoration of the symmetry despite the anomaly. For 2 light quark flavors the effective restoration of $U_A(1)$ is reflected in the degeneracy of the pion and the isovector-scalar $a_0(\delta)$ mass [46].
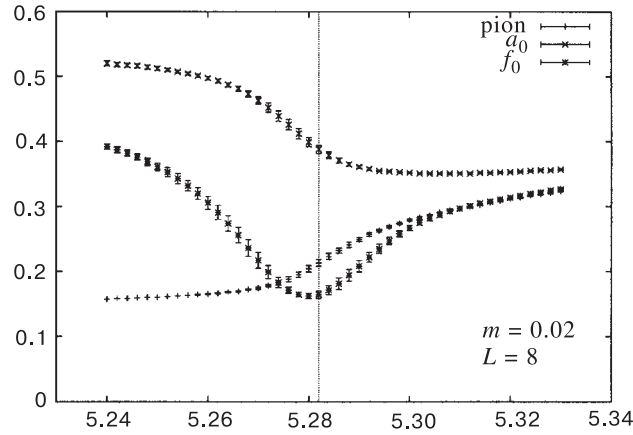
Fig. 10. Masses of π, a_0 and f_0 taken from the generalized susceptibilities, Eq. (38), for two flavors of staggered quarks as a function of the coupling. The critical coupling is indicated by the vertical line

This degeneracy can also be detected by comparing generalized susceptibilities defined via integrated propagators of a hadron H

$$\chi_H = \int d^4 x (\langle H(x) H^\dagger(0) \rangle) \sim \frac{1}{M_H^2}. \tag{38}$$

The susceptibilities have been computed by various groups [41, 47, 48] and a set of results is shown in Fig.10. At the critical temperature, π and f_0 become (almost) degenerate reflecting $SU_A(2)$ restoration while there remains a significant difference between a_0 and π in the investigated temperature range.

These results were obtained at finite quark mass and need to be extrapolated into the chiral limit. This was attempted in [47, 48]. Figure 11 shows the latest results by the Columbia group for the difference between π and a_0,

$$\omega = \int d^4 x (\langle \pi(x) \pi^\dagger(0) \rangle - \langle a_0(x) a_0^\dagger(0) \rangle). \tag{39}$$

If $U_A(1)$ is restored this quantity should vanish in the chiral limit. In the continuum, the susceptibility ω is expected to be an analytic and, for $N_F = 2$, even function in the quark mass. Indeed, fits with a quadratic m dependence work and lead to a finite intercept in the chiral limit. However, the data look strikingly linear and fitting them with a linear ansatz results in a vanishing of the susceptibility at $m = 0$. At finite lattice spacing, due to zero-mode shifts and perhaps also due to taking the square root of the determinant the approach towards the chiral limit is not so clear however [48]. Therefore one should continue to study
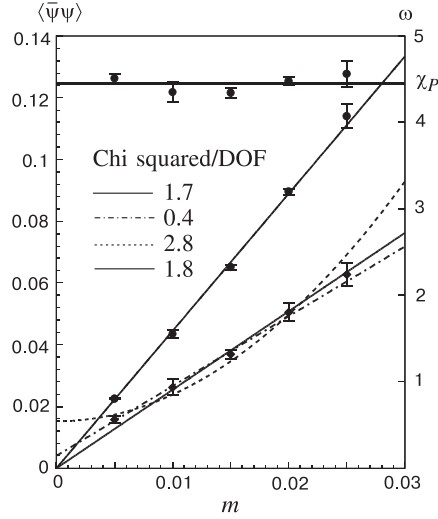
Fig. 11. The quantity ω, Eq. (39), which measures the breaking of the $U_A(1)$ symmetry plotted versus the quark mass (lowest data) together with various fits [48]. Also shown are the results for the integrated pion correlator, χ_P, and the chiral condensate. The data were obtained on a $16^3 \times 4$ lattice at fixed β slightly above β_c

the quark mass dependence at even smaller quark masses as well as at smaller lattice spacings.

The approach chosen in [49,50] is to determine screening masses. Above the critical temperature, the difference between π and a_0 mass drops considerably, but a nondegeneracy remains at finite quark mass, thus confirming the findings originating from the analysis of the susceptibilities. In order to address the problem of the chiral limit from a different angle, Ref. 50 also computed the lowest eigenvalues λ and corresponding eigenvectors ψ_λ of the fermion matrix D. In the continuum, in the phase symmetric with respect to the axial $SU(2)$, the chiral limit of ω is given by the zero-modes,

$$\omega = \langle \sum_{\lambda=0} \frac{\overline{\psi}_\lambda \gamma_5 \psi_\lambda}{i\lambda + m} \rangle. \qquad (40)$$

In [50] it is then verified that ω obtained from Eq. (39) is saturated by the contribution from low eigenmodes at finite a and m_q. Thus it seems that the continuum relation between the $U_A(1)$ and the eigenmodes is satisfied on the lattice. This supports that the vanishing of ω when the chiral limit is carried out at finite lattice spacing is caused by the absence of exact zero modes at finite a. Taking the continuum limit prior to the chiral one would therefore presumably

lead to nonvanishing ω. In this manner the results of [50] indicate that the $U_A(1)$ symmetry is not restored at the chiral transition.

4.3. Wilson Fermions $N_F = 2$. Wilson's discretization of the action for fermions breaks chiral symmetry explicitly. Therefore, the value for the hopping parameter κ which corresponds to the chiral limit is shifted away from its free field value $\kappa_c(\beta \to \infty) = 1/8$ to a coupling constant dependent $\kappa_c(\beta)$ which has to be tuned at each β value. At zero temperature one usually defines the chiral limit by means of the pion mass which vanishes according to

$$m_\pi^2 \approx \frac{1}{\kappa} - \frac{1}{\kappa_c}. \tag{41}$$

At sufficiently large temperatures this definition does not work anymore. For instance, at fixed and large enough β, when one lowers the quark mass by increasing κ, one reaches the transition to the plasma phase at which point the pion mass starts to increase because in the plasma phase the pion ceases to be a Goldstone particle and acquires a finite mass even in the limit of vanishing quark mass.

This results in the phase diagram as shown in Fig.12, which has been clarified by [51]. At finite N_τ, the line $\kappa_c(\beta)$ defined through the vanishing of the pion mass starts off at 1/4 at $\beta = 0$ and extends to $\kappa_c \simeq 0.22$ at about $\beta \simeq 4.0$ where it bends backwards again to the region of stronger couplings (see also [52]). On the other hand, coming from the confined phase, at the thermal line $\kappa_t(\beta)$
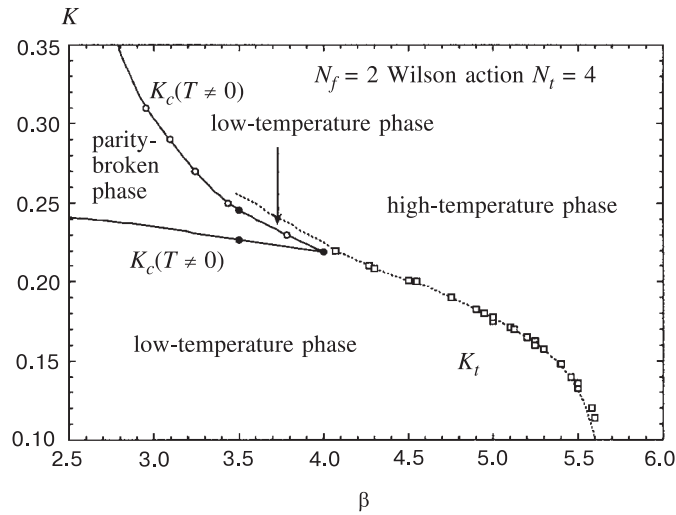

Fig. 12. The finite temperature phase diagram in the (β, κ) plane for standard Wilson fermions [51]

Scaling Analysis with O(4) Exponent
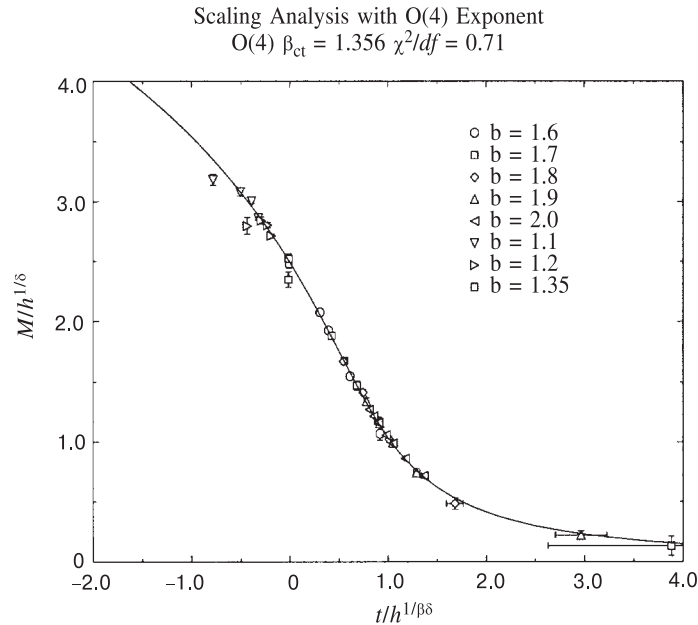O(4) $\beta_{ct} = 1.356$ $\chi^2/df = 0.71$

Fig. 13. The magnetic equation of state, Eq. (37), with two flavors of standard Wilson fermions on improved glue [54]. The various symbols denote data obtained at different values of the gauge coupling $b = 6/g^2$

where the Polyakov loop develops a nonvanishing expectation value the pion mass increases rapidly due to the approximate restoration of chiral symmetry. Only in the region where the thermal line is close to κ_c does the theory have a pion with a small mass. Thus, the chiral transition can only be explored in that region. Unfortunately, this region is at strong coupling for $N_\tau = 4$ and moves towards smaller coupling only very slowly with increasing temporal extent of the lattice [53], rendering a study of the transition in the vicinity of continuum physics prohibitively expensive. For that reason and for the well-known pathologies [34] several groups have started to work with improved actions.

In [54] the standard Wilson fermion action with RG-improved glue was simulated. Qualitatively, the phase diagram is very similar to the standard one so that small pion masses again are obtained in the vicinity of the finite temperature κ_c cusp. In addition to the phase diagram the group has also investigated the magnetic equation of state, Eq. (37). For Wilson fermions quark mass and chiral order parameter have to be obtained from chiral Ward identities [55]. This involves renormalization constants for which the lowest order perturbative values have been used in [54]. The results are shown in Fig.13. The agreement with

the $O(4)$ scaling curve is remarkable. The analysis was carried out on lattices of size $8^3 \times 4$ and with mainly not very small quark masses. It would be very interesting to continue the investigation on larger lattices and with more data at smaller quark masses.

4.4. More than 2 Flavors. The phase transition has also been studied for the number of flavors differing from 2. Regarding the nature of the chiral transition, for $N_F \geq 3$ and degenerate quark masses one expects first order in the continuum limit [35].

Early results in the staggered discretization (for a summary see, e.g., [56]) indeed show a behavior which is consistent with this expectation. Recently, the cases $N_F = 3$ and 4 with degenerate Wilson quarks have been studied in [57]. In both cases the phase diagram is very similar to the one with 2 flavors, in particular the κ_c line forms a cusp. At large quark masses, away from the cusp, one indeed observes first order behavior. When the quark mass is lowered however, the $N_F = 4$ data show a weakening of first-order signals. For $N_F = 3$ it seems that the first-order signal weakens when the discretization errors inherent to the approximate algorithm one has to use in this case are decreased. Thus, for both $N_F = 3$ and 4 Wilson quarks the order of the transition is still unclear.

The physically realistic case is the one of $N_F = 2 + 1$, meaning two flavors with almost vanishing mass and a strange quark about 25 times heavier. In the limit of a heavy strange quark the strange quark ceases to play a significant role in the chiral transition and one is approaching the two flavor case, hence expecting a second order transition. On the other hand, if up, down and strange quarks become degenerate (and light) one would expect the $N_F = 3$ transition with supposedly first order. The transition's nature thus depends crucially on the quark masses. The physical value of the quark mass is not easy to determine precisely in a lattice simulation. Moreover, running at about the physical value for the two light quarks is at best possible at strong coupling so far. Therefore, it is perhaps not too surprising that the two dedicated efforts to study the $2 + 1$ case, [58, 59], come to different conclusions. Ref. 58 is simulating staggered quarks and suggest a crossover or second order behavior while in the simulation with Wilson fermions [59] a first order behavior is favored. More work clearly is needed here.

5. EQUATION OF STATE

A quantitative understanding of the equation of state of QCD is one of the central goals in finite temperature field theory. The intuitive picture of the high temperature phase of QCD behaving like a gas of weakly interacting quarks and gluons is based on leading order perturbation theory. However, the well-known infrared problems of QCD result in a poor convergence of the perturbative
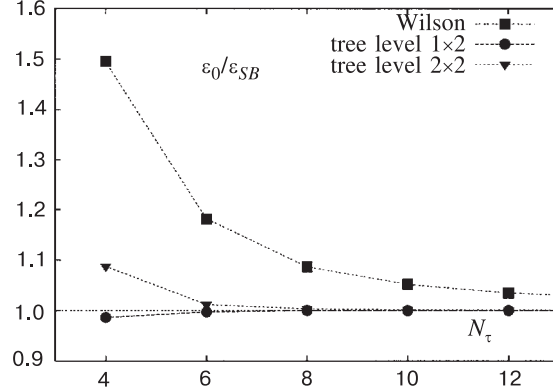
Fig. 14. The gluonic part of the energy density in the infinite temperature limit, computed on lattices with finite temporal extent and normalized to the continuum Stefan — Boltzmann value, for various gauge actions [65]

expansion of the thermodynamic potential even at temperatures very much higher than T_c [60].

Lattice calculations of energy density (ϵ), pressure (p) and other thermodynamic variables at high temperature, on the other hand, are hampered by ultraviolet cut-off effects. As these quantities receive substantial contributions from high momentum modes $\sim T$ the effects of finite lattice spacings can be large. For instance, the energy density in the infinite temperature limit deviates considerably from the continuum Stefan-Boltzmann value. For the pure gauge theory in the standard Wilson discretization the corrections are

$$\epsilon_0^G = \epsilon_{SB}^G \left[1 + \frac{10}{21}\left(\frac{\pi}{N_\tau}\right)^2 + \frac{2}{5}\left(\frac{\pi}{N_\tau}\right)^4 + \mathcal{O}\left(\left(\frac{\pi}{N_\tau}\right)^6\right)\right]. \qquad (42)$$

Recall that $\pi/N_\tau = \pi T a$. As can be seen from Fig.14 the corrections can be as large as 50 % for $N_\tau = 4$. On the other hand, the nonperturbative determination of, e.g., the pressure makes use of the following formula [61]

$$\left.\frac{p}{T^4}\right|_{g_0}^g \equiv -\left.\frac{f}{T^4}\right|_{g_0}^g = N_\tau^4 \int_{6/g_0^2}^{6/g^2} \mathrm{d}(6/g'^2)(S_0 - S_T), \qquad (43)$$

where S_0 is the expectation value of the action at zero and S_T the same quantity at finite temperature. From Eq. (43) it is clear that the signal decreases $\sim 1/N_\tau^4$ with increasing N_τ, i.e., decreasing a.

In order to determine quantitatively the size of the deviation of the energy density or pressure from the ideal gas value an extrapolation to the continuum limit
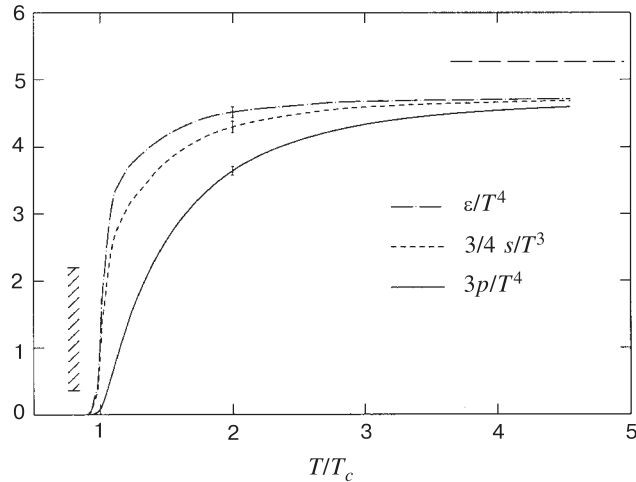
Fig. 15. The extrapolated continuum limit of energy density, entropy density and pressure in the pure glue theory [2]. The dashed horizontal line shows the ideal gas limit. The hatched vertical band indicates the size of the discontinuity in ϵ/T^4 (latent heat) at T_c [62]

is mandatory. The result of such an extrapolation for the pure gauge theory [2] is shown in Fig.15. The energy density rapidly rises to about 85 % of the ideal gas value at $2T_c$ and then shows a rather slow increase which is consistent with a logarithmic behavior as one would expect from a leading order perturbative correction. The pressure rises much more slowly near T_c and even at $T \simeq 3T_c$ shows sizeable deviations from the ideal gas relation $\epsilon = 3p$.

As stated in section 2, improved actions aim at reducing the differences between the continuum and lattice action due to finite lattice spacings. Since the pressure is related to the action, Eq. (43), any improvement in the action will reduce the finite lattice spacing effects on the high-momentum contribution to, e.g., the pressure in the ideal gas limit. This is indicated in Fig.14, where the analytical results in the infinite temperature limit for some improved actions are compared with the standard action. As can be seen, by use of an improved action the finite a corrections can be brought down to the level of a few per cent already at temporal extents of $N_\tau = 4$.

The improvement seems to work not only in the high temperature limit but also already close to T_c. Figure 16 summarizes the results of numerical simulations of a variety of improved actions [67]. Although the lattice extent in the temporal direction was only 4, the improved actions lead to values quite close to the continuum extrapolation of the standard action results. This in turn gives strong support to the continuum extrapolation presented above. Tree-level improvement seems to be the leading effect, although one would have

p/T^4

$4_{(1\times1)}$

cont

$4_{(2\times2)}$

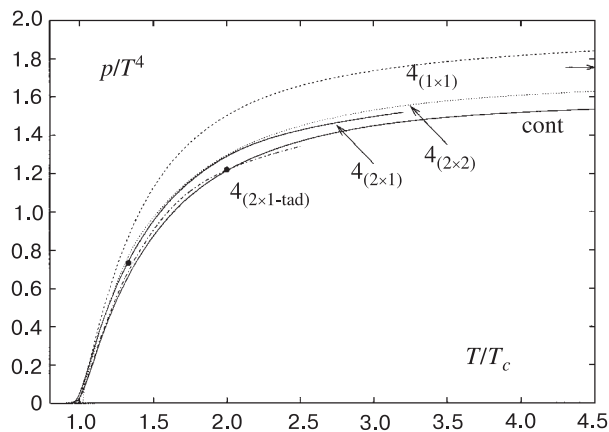$4_{(2\times1)}$

$4_{(2\times1\text{-tad})}$

T/T_c

Fig. 16. The pressure in SU(3) pure gauge theory on lattices with $N_\tau = 4$ for various actions [67] indicated by the subscripts. The solid line shows the continuum extrapolation obtained from the standard plaquette action. The dots result from a calculation with a classical fixed point action on a lattice with $N_\tau = 3$ [87]

e/T^4, $3P/T^4$

Fit using O(4) scaling

$am_q = 0.0 \rightarrow$

$\leftarrow 0.0125$
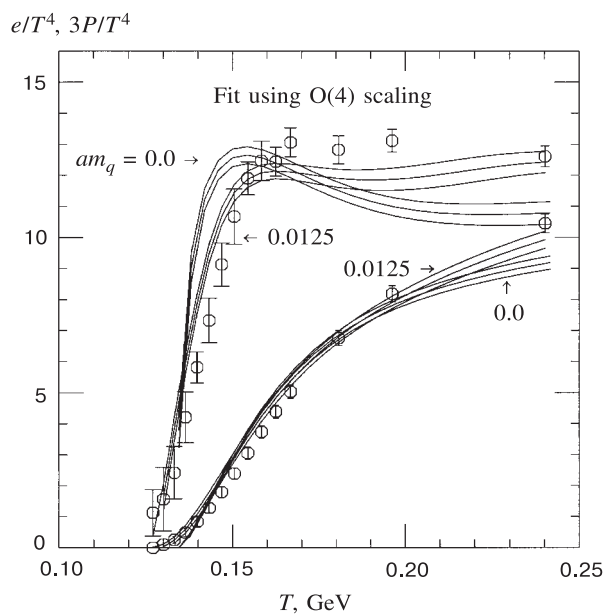
$0.0125 \rightarrow$

$\uparrow$
0.0

T, GeV

Fig. 17. Energy density and pressure from a simulation with the 2 flavor staggered standard action. The results are extrapolated to the chiral limit by means of an $O(4)$ ansatz. Fit and data at the lowest quark mass $ma = 0.0125$ are also shown. The triplets of curves represent the central value and the one standard deviation error [64]
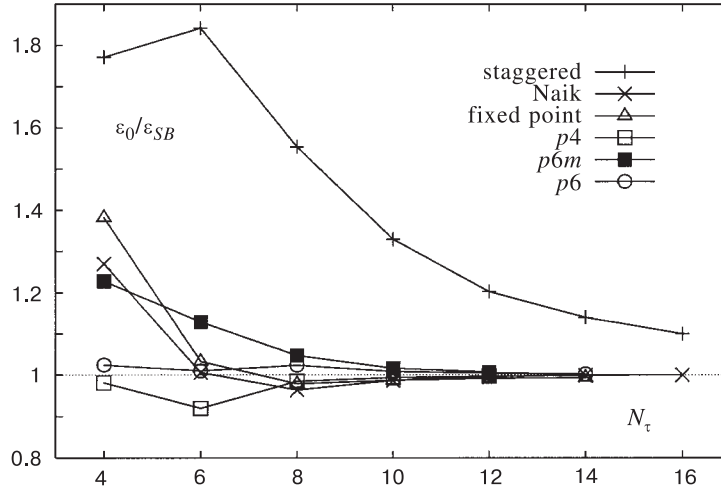
Fig. 18. The fermionic part of the energy density in the infinite temperature limit, computed on lattices with finite temporal extent and normalized to the continuum Stefan — Boltzmann value, for various staggered fermion actions [66]

expected that close to the transition infrared modes and their improvement would be more important. Tadpole improvement has an effect though for the interface tension [68].

The equation of state has also been investigated with dynamical quarks in the staggered discretization. For two flavors the standard action was used on lattices with temporal extent $N_\tau = 4$ and 6 [63, 64]. The data for the energy density on the $N_\tau = 4$ lattices showed an overshooting above the ideal gas limit at temperatures just above T_c. This bump is not present anymore in the newest data for $N_\tau = 6$ and at the smallest quark mass, Fig.17. The extrapolation to the chiral limit shown in this figure does have a peak again but this effect is attributed to an artefact of the extrapolation.

The extrapolation to the continuum limit, however, is difficult with the (fermionic) standard action. The finite lattice spacing corrections in the high temperature limit are large

$$\epsilon_0^F = \epsilon_{SB}^F \left[1 + \frac{465}{441} \left(\frac{\pi}{N_\tau} \right)^2 + \mathcal{O}\left(\left(\frac{\pi}{N_\tau} \right)^4 \right) \right] \tag{44}$$

and only very slowly decreasing with N_τ as can also be seen from Fig.18 [66]. This makes analyses based on improved actions even more desirable than in the quenched case. Indeed, in the high temperature limit, the deviations from the continuum Stefan — Boltzmann prediction can be brought down to the level of less than 10 % at $N_\tau = 4$, Fig.18.
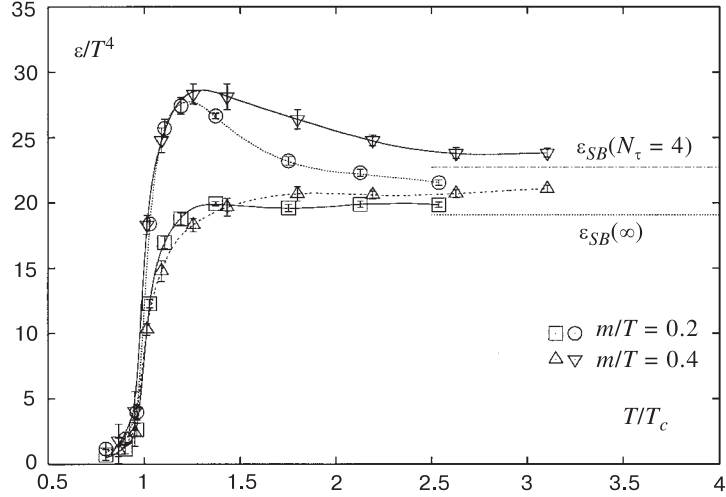
Fig. 19. Energy density for 4 flavors of quarks, obtained from a calculation at $N_\tau = 4$ with an improved action [25]. The upper two curves show the energy density at the given quark masses, the lower set is obtained by neglecting the contribution to the energy density which is proportional to the quark mass and vanishes in the chiral limit. The horizontal lines give the ideal gas limit at $N_\tau = 4$ and in the continuum limit

A first attempt to analyze bulk thermodynamic quantities in the vicinity of T_c by means of simulations with an improved fermion discretization scheme, the Naik action, has been carried out in [25]. The results are shown in Fig.19.

At the moment, there are investigations under way which try to estimate the effect of various improvement strategies on the restoration of flavor symmetry [66, 69–71]. It remains to be seen how much this can help to extract energy density or pressure closer to the continuum limit at finite temperatures.

6. SCREENING LENGTHS AND MASSES

An important goal of analytical as well as lattice investigations has been to understand the nature of excitations characterizing the structure of hot QCD in the vicinity of the transition and in the plasma phase. At high temperature, due to asymptotic freedom the effective coupling constant $g(T)$ should become small and one is lead to expect that the plasma consists of a gas of only weakly interacting quarks and gluons. On the other hand, there are indications that even at high temperatures the excitation spectrum might be more complicated in particular because of nonperturbative effects in the chromomagnetic sector of QCD.

The definition of a chromoelectric and a chromomagnetic mass beyond perturbation theory is somewhat ambiguous. A possible choice is to extract the chromoelectric or Debye mass from the heavy quark potential. At the deconfinement temperature the potential between heavy, nonrelativistic quarks changes from a linear rising, confining form to a screened Coulombic behavior,

$$V(R) \sim T \left(\frac{g^2}{R}\right)^2 \exp\{-2m_e R\}, \tag{45}$$

which is obtained from two-gluon exchange in resumed lowest order perturbation theory. Here, m_e denotes the Debye-mass, for which (lowest order) perturbation theory predicts

$$m_{e0} = \sqrt{\frac{N_c}{3} + \frac{N_F}{6}} \, gT. \tag{46}$$

The (color averaged) heavy quark potential is obtained from Polyakov loop correlations,

$$V_{av}(\vec{x}) = -T \ln \frac{\langle \, L(\vec{x}) \; L(\vec{0}) \, \rangle}{\langle \, L \, \rangle^2}, \tag{47}$$

with $L(\vec{x})$ being the Polyakov loop at spatial coordinates $\vec{x}$, see Eq. (29). Indeed, the potential data [72] show the anticipated decrease in the linear rise, i.e. the string tension decreases, when the critical temperature is approached from below, see Fig. 20. Above T_c screening $\sim exp(-\mu R)$ clearly is observed. Moreover, comparing the potentials at different temperatures, one can verify that the screening mass μ depends on the temperature as $\mu \sim T$. However, when analyzed in detail, the data does not follow Eqs. (45),(46) in so far neither the power 2 of the Coulomb term nor the prediction for the coefficient in the exponential is observed. One might conclude that at the temperatures investigated the behavior of the Polyakov loop correlations is not described properly by simple perturbation theory.

For an alternative definition of the effective gluon masses at high temperature one can refrain to the exponential decrease of a gluon-gluon correlation function. That enables one to distinguish between the electric sector defined via

$$G_e(x) = \langle A_0(x) A_0(0) \rangle \tag{48}$$

and the magnetic one ($k = 1, 2, 3$)

$$G_m(x) = \langle A_k(x) A_k(0) \rangle, \tag{49}$$

where $A_\mu, \mu = 0, .., 3$ denotes the gluon field. The gluon correlation function is gauge variant so that one has to fix to a definite gauge, usually the Landau gauge.
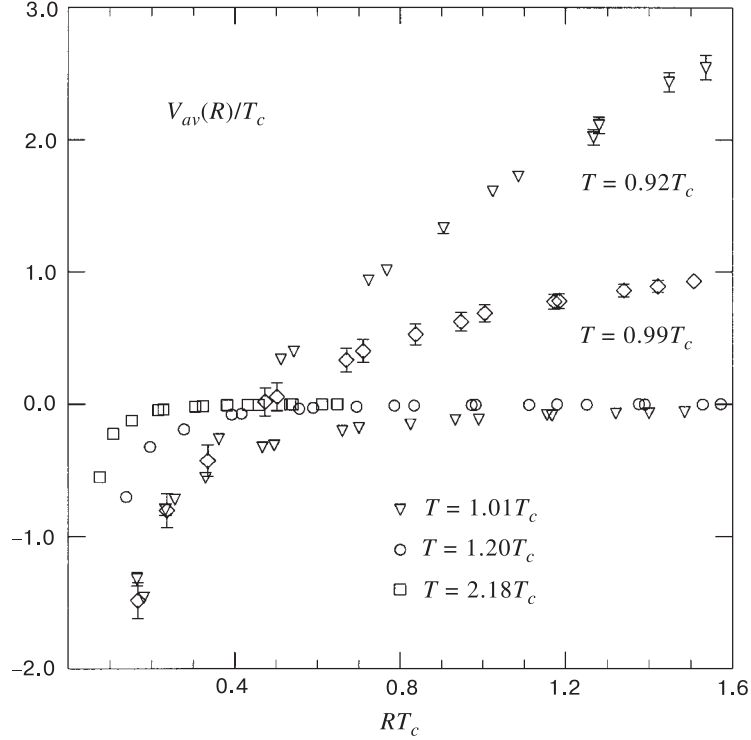
Fig. 20. The heavy quark potential of the pure glue theory at various temperatures below the phase transition and in the deconfined phase

The correlation functions (48),(49) have been analyzed in the simpler color group $SU(2)$ [73]. In the magnetic sector, a nonvanishing chromomagnetic gluon mass with a temperature variation of $m_m(T) \simeq 0.5g^2(T)T$ was found. Such a mass is widely expected and cures the well-known infrared problems of high temperature perturbation theory at this order. If m_m is nonvanishing next-to-leading order perturbation theory, then predicts [74] for the electric mass

$$m_e^2 = m_{e0}^2 \left(1 + g\frac{N}{2\pi}\sqrt{\frac{6}{2N+N_F}}[\ln\frac{2m_e}{m_m} - \frac{1}{2}] \right), \qquad (50)$$

where m_{e0} denotes the leading term, Eq. (46). The results of [73] show that at best at very high temperatures of $\mathcal{O}(10^4 T_c)$ contact can be made with this prediction, Fig. 21. In general, the data can be described by the formula $\sqrt{1.7}g(T)T$ indicating that the screening mechanism is a highly nonperturbative effect even at large temperatures.
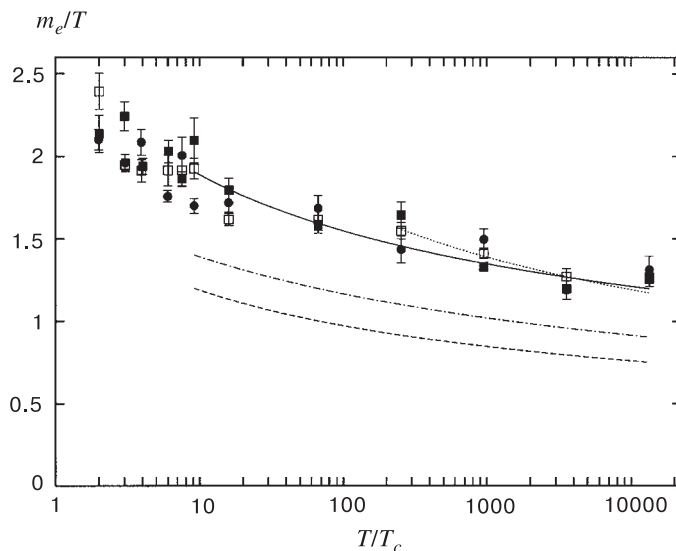
Fig. 21. The electric gluon mass in units of the temperature versus T/T_c [73]. Squares denote results from simulations with the standard Wilson action at two different lattice volumes, the circles originate from a simulation with an improved action. The lines represent analytic predictions at tree level, Eq. (46) (dashed) and at next-to-leading order, Eq. (50) with a magnetic mass determined in the same simulation (dashed-dotted) or fit results with an ansatz $m_e = const \times g(T)T$ (solid) and an ansatz summarizing ad hoc higher contributions to Eq. (50) (dotted)

A third definition for the (electric) screening mass is applied in [75]. Here the Debye mass is extracted from the correlation of a gauge-invariant operator [76] which is odd under the Euclidean equivalent of time reversal and charge conjugation. Moreover, [75] apply dimensional reduction and simulate the 3rd effective theory. Although the results quantitatively differ somewhat from those of [73] the conclusion is the same in both cases.

Hadron correlation functions at high temperature but below the transition are interesting for phenomenological reasons. For instance, a temperature dependent ρ meson mass and width could perhaps explain the dilepton spectra found in nucleus-nucleus collisions at high energy. Detailed lattice investigations (of spatial correlators, see below) have been carried out in the quenched approximation so far [77]. Based on the staggered fermion discretization, these studies show that the investigated quantities remain unaffected by the temperature up to T_c. Some recent work with Wilson fermions confirms this observation, although at one temperature value only so far [78]. As these analyses work in the quenched approximation where the transition has been determined to be of first order, dy-

namical quarks could alter that picture somewhat because in this case a continuous transition is expected.

Correlation functions of operators with the quantum numbers of hadrons have, in the plasma phase, been investigated in a variety of papers. Due to the limited extent of the lattice in the temporal direction $0 \leq x_0 \leq 1/T$ one cannot study the correlations at large time separations which is what one would like to do in order to isolate the contribution of the state with the lowest energy or mass. Therefore, one usually focussed on the long distance behavior of spatial correlators

$$\langle H(z)H^\dagger(0)\rangle \sim \exp(-M_{\rm sc}z) \tag{51}$$

which decay with the screening mass $M_{\rm sc}$. (For exceptions see [79, 80].) These screening masses would coincide with the masses if the zero temperature dispersion relation were applicable. In any case, the spatial correlators depend on the same spectral density as the masses and thus deliver information about it. As noted above, at sufficiently high temperature one expects that the plasma consists of a gas of weakly interacting quarks and gluons. In this case, the spatial correlation function should be described by the exchange of two (almost) free quarks. Since quarks propagating in the spatial direction carry nonvanishing "momenta" of $(2n+1)\pi T$ because they obey antiperiodic boundary conditions in the temporal direction, the minimum contribution to the correlator is given by

$$M_{\rm sc} = l\sqrt{m_q^2 + (\pi T)^2} \tag{52}$$

in the continuum limit, where $l = 2$ for mesons and $l = 3$ for baryons. Indeed, lattice results [81] in the vector and axial vector channel as well as for baryonic excitations are compatible with this expectation, see Fig. 22. However, the scalar and pseudoscalar channels show substantial deviations. This might indicate the existence of bound states as bosonic bound states would have vanishing Matsubara frequencies and hence could have a lower screening mass. Also, one could have substantial spin dependent interactions.

On the other hand, the spatial wave functions of the states contributing to the spatial correlator, Eq. (51), were analyzed [82]. Here one finds the same behavior as at zero temperature, an exponential decay which is not expected from leading order perturbation theory and which suggests that the relevant hadronic excitations are bound states also in the plasma phase, at least at temperatures just above T_c. According to [83], this behavior could be explained by the fact that the dimensionally reduced, 3-D effective theory and correspondingly spatial Wilson loops in 3+1 dimensions [84] show confinement. Solving then a two-dimensional Schrödinger equation with a potential which includes a temperature-dependent (spatial) string tension leads to spatial wavefunctions

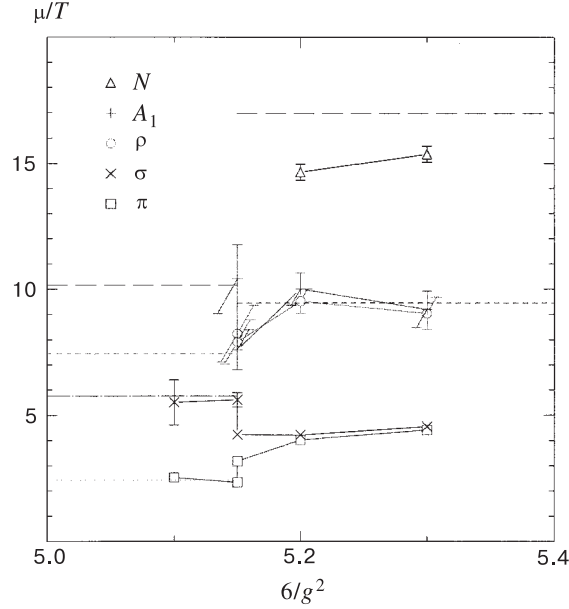$$|\psi(R)| \sim \exp(-\sqrt{\sigma_{\rm spat}(T)\pi T}R^{3/2}) \tag{53}$$

Fig. 22. A representative set of hadronic screening masses [81] from a staggered 4 flavor simulation. The masses are plotted versus the gauge coupling across the transition at $6/g^2 \simeq 5.15$. The lines to the left indicate the zero temperature values for the masses, the lines to the right show the expectation for free quarks, $\mu/T = 2\pi$ and 3π for mesons and baryons respectively, corrected for finite lattice effects

and to screening masses, which differ from Eq. (52) by terms of $\mathcal{O}(\sqrt{\sigma_{\mathrm{spat}}(T)})$. A quantitative test of this suggestion is not yet available though.

Finally, heavy quarks in the range $m_c < m < m_b$ at temperatures around the critical one have for the first time been investigated in [85]. The heavy quarks are simulated by means of a nonrelativistic approximation to QCD [86], applied to quenched configurations. The propagation of quarkonia states is followed in the time direction. For that purpose, the investigation is carried out on anisotropic lattices with a large anisotropy ratio $\xi = a_\sigma/a_\tau = 4.65$ in order to have enough Matsubara frequencies. So far, the analysis was done for the $^3S_1$ ground and first excited state. Below T_c, at about $0.8T_c$ no temperature effect was seen. At $1.2T_c$, the propagator which is dominated by the ground state at large time separations t from the source becomes flatter than the zero temperature propagator at large t. This effect can be interpreted as a decrease in the mass by a small amount of about 12 MeV at the lightest quark mass simulated. The effect becomes weaker with increasing quark mass. The first excited state, projected on by the same trial wave function as at $T = 0$, undergoes a larger change of about - 240 MeV at the

charm quark mass. Thus, at least qualitatively, the results are in accord with the expectations from a Debye-screened potential model, namely that smaller states feel the screening less.

7. CONCLUSIONS

In these lectures, the current status of lattice investigations of QCD at finite temperature has been reviewed. Bulk properties of the pure gluon system are known to rather high precision. Thus, the emphasis of these studies recently has shifted towards simulations of the full theory including dynamical fermions.

At currently accessible quark masses, these investigations have led to an estimate for the critical temperature for 2 flavors of around 150 MeV. This number is almost a factor of two smaller than the quenched value of 270(5) MeV. Thus, at fixed temporal extent of the lattice, simulations of full QCD in the vicinity of the critical temperature have to be carried out at considerably larger lattice spacings than in the quenched case.

Analyses of the critical behavior at the chiral transition suggest a second order transition. However, at present the estimates for the critical exponents are in disagreement with theoretical expectations. This holds for simulations in the staggered discretization of quarks while first results with Wilson fermions seem to support the anticipated universality with $O(4)$. Concerning the anomalous axial $U(1)$, at present it is not yet entirely clear whether or not this symmetry is effectively restored at the chiral transition. Further studies at smaller quark mass values are required to shed more light on these important issues.

In addition, lattice results of investigations of various screening lengths have been presented. At temperatures which are accessible in present and future heavy ion collision experiments the data consistently show sizable deviations from simple perturbative expectations. Nonperturbative effects therefore need to be taken into account in the interesting temperature range.

This also holds for energy density and pressure. Moreover, analytic studies of the infinite temperature limit of these quantities on finite lattices reveal discretization effects which are particularly large in the fermionic part of the energy density if standard discretizations of the fermion action are used. This, together with the observation of a small value of the critical temperature in two-flavor QCD has stimulated activities to explore improved actions also in the context of finite temperature studies.

8. ACKNOWLEDGEMENTS

REFERENCES

1. **Ukawa A.** — Nucl. Phys. B (Proc.Suppl.), 1990, v.17, p.118 and references therein.

2. **Boyd G. et al.** — Phys. Rev. Lett., 1995, v.75, p.4169; Nucl. Phys., 1996, v.B469, p.419.

3. **Iwasaki Y. et al.** — Phys. Rev., 1997, v.D56, p.151.

4. **Beinlich B. et al.** — hep-lat/9707023.

5. **Wilson K.** — Phys. Rev., 1974, v.D10, p.2445.

6. **Nielsen H.R., Ninomiya M.** — Nucl. Phys., 1981, v.B193, p.173.

7. **Kogut J.B., Susskind L.** — Phys. Rev., 1975, v.D11, p.395.

8. **Metropolis N. et al.** — J. Chem. Phys., 1953, v.21, p.1087.

9. **Duane S. et al.** — Phys. Lett., 1987, v.B195, p.216.

10. For an alternative algorithm see **Lüscher M.** — Nucl. Phys., 1994, v.B418, p.637.

11. **Gottlieb S. et al.** — Phys. Rev., 1987, v.D35, p.2531.

12. For overviews see, e.g., **Ph.de Frocrand** — Nucl. Phys. B (Proc.Suppl.), 1996, v.47, p.228; **Frommer A.** — Nucl. Phys. B (Proc.Suppl.), 1997, v.53, p.120.

13. **Symanzik K.** — Nucl. Phys., 1983, v.B226, p.187; ibid p.205.

14. **Lüscher M., Weisz P.** — Comm. Math. Phys., 1985, v.97, p.19; Phys. Lett., 1985, v.B158, p.250.

15. **Lepage G.P., Mackenzie P.B.** — Phys. Rev., 1993, v.D48, p.2250.

16. **Sheikholeslami B., Wohlert R.** — Nucl. Phys., 1985, v.B259, p.572.

17. **Naik S.** — Nucl. Phys., 1989, v.B316, p.238.

18. **Lüscher M. et al.** — Nucl. Phys., 1997, v.B491, p.323.

19. For a recent overview see **Hasenfratz P.** — Nucl. Phys. B (Proc.Suppl.), 1998, v.63, p.53.

20. **Ukawa A.** — Nucl. Phys. B (Proc. Suppl.), 1997, v.53, p.106.

21. **Cella G. et al.** — Phys. Lett., 1994, v.B333, p.457.

22. **Legeland C. et al.** — Nucl. Phys. B (Proc.Suppl.), 1998, v.63, p.260.

23. **MILC Collaboration** — Phys. Rev., 1997, v.D56, p.5584.

24. **Bielefeld results,** unpublished.

25. **Engels J. et al.** — Phys. Lett., 1997, v.B396, p.210.

26. **Born K.D. et al.** — Phys. Lett., 1994, v.B329, p.325.

27. **Bernard C. et al.** — Phys. Rev., 1996, v.D54, p.4585.

28. **Gottlieb S. et al.** — Phys. Rev.Lett., 1987, v.59, p.1513.

29. **Bernard C. et al.** — Phys. Rev., 1992, v.D45, p.3854.

30. **HTMCGC Collaboration** — Phys. Rev., 1993, v.D47, p.3619; Nucl.Phys. B (Proc.Suppl.), 1993, v.30, p.315.

31. **Mawhinney R.** — Nucl. Phys. B (Proc.Suppl.), 1993, v.30, p.331.

32. **Bitar K.M. et al.** — Phys. Rev., 1991, v.D43, p.2396.

33. **Bernard C. et al.** — Phys. Rev., 1992, v.D46, p.4741.

34. **Blum T. et al.** — Phys. Rev., 1994, v.D50, p.3377.

35. **Pisarski R.D., Wilczek F.** — Phys. Rev., 1984, v.D29, p.338;
    Wilczek F. — Int. J. Mod. Phys., 1992, v.A7, p.3911;
    Rajagopal K., Wilczek F. — Nucl. Phys., 1993, v.B399, p.395.

36. **Karsch F.** — Phys. Rev., 1993, v.D49, p.3791.

37. **Baker G.A., Nickel B.G., Meiron D.I.** — Phys. Rev., 1978, v.B17, p.1365;
    Le Guillou J.C., Zinn-Justin J. — Phys. Rev., 1980, v.B21, p.3976;
    Kanaya K., Kaya S. — Phys. Rev., 1995, v.D51, p.2404.

38. **Kocić A., Kogut J.B.** — Phys. Rev. Lett., 1995, v.75, p.3109; Nucl. Phys., 1995, v.B455, p.229.

39. **Karsch F., Laermann E.** — Phys. Rev., 1994, v.D50, p.6954.

40. **JLQCD Collaboration** — Nucl. Phys. B (Proc.Suppl.), 1998, v.60, p.188; ibid. 1998, v.63, p.403.

41. **Laermann E.** — Nucl. Phys. B (Proc.Suppl.), 1998, v.60, p.180.

42. **Fukugita M. et al.** — Phys. Rev. Lett., 1990, v.65, p.816; Phys. Rev., 1990, v.D42, p.2936;
    Brown F.R. et al. — Phys. Rev. Lett., 1990, v.65, p.2491.

43. **DeTar C.** — Nucl. Phys. B (Proc. Suppl.), 1995, v.42, p.73.

44. **Toussaint D.** — Phys. Rev., 1997, v.D55, p.362.

45. **DeTar C. et al.** — Nucl. Phys. B (Proc.Suppl.), 1998, v.63, p.400; see also
    Toussaint D. et al. — Nucl. Phys. B (Proc.Suppl.), 1998, v.60, 1998, p.195.

46. **Shuryak E.V.** — Comments Nucl. Phys., 1994, v.21, p.235;
    Lee S.H., Hatsuda T. — Phys. Rev., 1996, v.D54, p.1871;
    Evans N., Hsu S.D.H., Schwetz M. — Phys. Lett, 1996, v.B375, p.262;
    Birse M.C., Cohen T.D., McGovern J.A. — Phys. Lett., 1996, v.B388, p.137.

47. **Bernard C.B. et al.** — Phys. Rev. Lett., 1997, v.78, p.598.

48. **Christ N.** — Nucl. Phys. B (Proc.Suppl.), 1998, v.60, p.203.

49. **Gottlieb S. et al.** — Phys. Rev., 1997, v.D55, p.6852.

50. **Kogut J.B., Lagaë J.-F., Sinclair D.K.** — hep-lat/9801020.

51. **Aoki S., Ukawa A., Umemura T.** — Phys. Rev. Lett., 1996, v.76, p.873 and references therein.

52. **Bitar K.** — Phys. Rev., 1997, v.D56, p.2736.

53. **Iwasaki Y. et al.** — Phys. Rev., 1996, v.D54, p.7010.

54. **Iwasaki Y. et al.** — Phys. Rev. Lett., 1997, v.78, p.17.

55. **Bochicchio M. et al.** — Nucl. Phys., 1985, v.B262, p.331;
    Itoh S. et al. — Nucl. Phys., 1986, v.B274, p.33.

56. **Gottlieb S.** — Nucl. Phys. B (Proc.Suppl.), 1991 v.20, p.247.

57. **Aoki S.** — Nucl. Phys. B (Proc.Suppl.), 1998, v.60, p.206 and references therein;
    Aoki S. et al. — private communication.

58. **Brown F.R. et al.** — Phys. Rev. Lett., 1990, v.65, p.2491.

59. **Iwasaki Y. et al.** — Phys. Rev., 1996, v.D54, p.7010.

60. **Arnold P., Zhai C.-X.** — Phys. Rev., 1994, v.D50, p.7603.

61. **Engels J., Karsch F., Redlich K.** — Nucl. Phys., 1995, v.B435, p.295.

62. **Iwasaki Y. et al.** — Phys. Rev., 1992, v.D46, p.4657.

63. **MILC Collaboration** — Phys. Rev., 1995, v.D51, p.5153.

64. **MILC Collaboration** — Phys. Rev., 1997, v.D55, p.6861.

65. **Karsch F.** — Nucl. Phys. B (Proc.Suppl.), 1998, v.60, p.169.

66. **Peikert A. et al.** — Nucl. Phys. B (Proc.Suppl.), 1998, v.63, p.895.

67. **Beinlich B. et al.** — Nucl. Phys. B (Proc.Suppl.), 1998, v.63, p.922.

68. **Beinlich B., Karsch F. Peikert A.** — Phys. Lett., 1997, v.B390, p.268.

69. **Luo Y.** — Phys. Rev., 1998, v.D57, p.265.

70. **Lagaë J.-F., Sinclair D.** — Nucl. Phys. B (Proc.Suppl.), 1998, v.63, p.892.

71. **Blum T. et al.** — Phys. Rev., 1997, v.D55, p.1133.

72. **Laermann E. et al.** — Nucl. Phys. B (Proc.Suppl.), 1995, v.42, p.120.

73. **Heller U., Karsch F., Rank J.** — Phys. Rev., 1998, v.D57, p.1438.

74. **Rebhan A.K.** — Phys. Rev., 1993, v.D48, p.R3967.

75. **Kajantie K. et al.** — Nucl. Phys., 1997, v.B503, p.357.

76. **Arnold P., Yaffe L.G.** — Phys. Rev., 1995, v.D52, p.7208.

77. **Gupta S.** — Phys. Lett., 1991, v.B288, p.171;
    Boyd G. et al. — Phys. Lett., 1995, v.B349, p.170.

78. **Schmidt P., Laermann E.** — Nucl. Phys. B (Proc.Suppl.), 1998, v.63, p.391.

79. **Hashimoto T., Nakamura T., Stamatescu I.O.** — Nucl. Phys., 1993, v.B400, p.267.

80. **Boyd G. et al.** — Z. Phys., 1994, v.C64, p.331.

81. **Gocksch A., Rossi P., Heller U.M.** — Phys. Lett., 1988, v.B205, p.334;
    Gottlieb S. et al. — Phys. Rev. Lett., 1987, v.59, p.1881;
    DeTar C., Kogut J.B. — Phys. Rev. Lett., 1987, v.59, p.399;
    Born K.D. et al. — Phys. Rev. Lett., 1991, v.67, p.302.

82. **Bernard C. et al.** — Phys. Rev. Lett., 1992, v.68, p.2125.

83. **Koch V. et al.** — Phys. Rev., 1992, v.D46, p.3169.

84. **Borgs C.** — Nucl. Phys., 1985, v.B261, p.455;
    Manousakis E., Polonyi J. — Phys. Rev. Lett., 1987, v.58, p.847;
    Karsch F., Laermann E., Lütgemeier M. — Phys. Lett., 1995, v.B346, p.94.

85. **Fingberg J.** — hep-lat/9707012.

86. **Davies C.T.H. et al.** — Phys. Rev., 1995, v.D52, p.6519.

87. **Papa A.** — Nucl. Phys., 1996, v.B478, p.335.